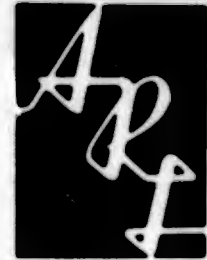


AD617891

ARL 65-90  
MAY 1965

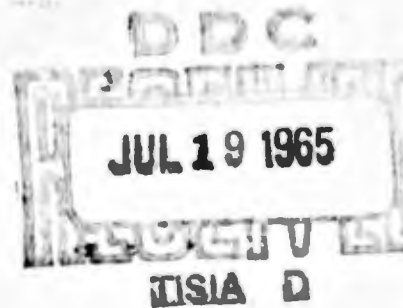


# Aerospace Research Laboratories

## MASS INJECTION IN A HYPERSONIC CAVITY FLOW

KENNETH M. NICOLL  
PRINCETON UNIVERSITY  
PRINCETON, NEW JERSEY

COPY _____	OF _____	<i>ku</i>
HARD COPY	\$ .300	
MICROFICHE	\$ .75	
<i>80-P</i>		



**OFFICE OF AEROSPACE RESEARCH**  
**United States Air Force**



**ARCHIVE COPY**

**NOTICES**

When Government drawings, specifications, or other data are used for any purpose other than in connection with a definitely related Government procurement operation, the United States Government thereby incurs no responsibility nor any obligation whatsoever; and the fact that the Government may have formulated, furnished, or in any way supplied the said drawings, specifications, or other data, is not to be regarded by implication or otherwise as in any manner licensing the holder or any other person or corporation, or conveying any rights or permission to manufacture, use, or sell any patented invention that may in any way be related thereto.

. . . . .

Qualified requesters may obtain copies of this report from the Defense Documentation Center, (DDC), Cameron Station, Alexandria, Virginia.

. . . . .

This report has been released to the Office of Technical Services, U. S. Department of Commerce, Washington 25, D. C. for sale to the general public.

. . . . .

Copies of ARL Technical Documentary Reports should not be returned to Aerospace Research Laboratories unless return is required by security considerations, contractual obligations or notices on a specified document.

**BLANK PAGE**

**ARL 65-90**

**MASS INJECTION IN A HYPERSONIC  
CAVITY FLOW**

**KENNETH M. NICOLL  
PRINCETON UNIVERSITY  
PRINCETON, NEW JERSEY**

**MAY 1965**

**Contract AF 33(615)-1079  
Project No. 7063  
Task No. 70i3-03**

**AEROSPACE RESEARCH LABORATORIES  
OFFICE OF AEROSPACE RESEARCH  
UNITED STATES AIR FORCE  
WRIGHT-PATTERSON AIR FORCE BASE, OHIO**

## FOREWORD

This research was carried out as part of a program on hypersonic flows sponsored by the Aerospace Research Laboratories, Office of Aerospace Research, United States Air Force, under Contract AF 33(615)-1079, monitored by Dr. Robert H. Korkegi.

The author would like to acknowledge gratefully the advice and help received from Prof. S. M. Bogdonoff during the course of this work.

## ABSTRACT

The present report describes an experimental investigation of a hypersonic cavity flow with mass-injection into the separated-flow region. The experiments were carried out in a helium wind-tunnel at a free-stream Mach number of eleven. The injected gas was helium. Two parameters were varied during the study -- the mass injection rate and the height of the separation shoulder relative to the reattachment shoulder. The effects of these parameters on the distributions of pressure and heat transfer rate were investigated.

Mass injection appeared to have no drastic effect on transition Reynolds number, and the cavity flow is believed to have been laminar throughout the present investigation. The effect on the cavity floor pressure of raising the separation shoulder relative to the reattachment shoulder was of the same order as the effect of mass injection, the two effects being virtually independent of one another. However, the flow in the immediate vicinity of the reattachment shoulder and downstream was primarily controlled by mass injection rate. Small amounts of mass injection were capable of completely removing the pressure peak at reattachment, and could produce a flow with almost constant pressure within and downstream of the cavity. Mass injection had a pronounced effect on the heat transfer rate in the vicinity of reattachment, and reductions of as much as a factor of six were obtained in the heat transfer peak in this region. Furthermore, the heat transfer rates up to about one cavity length downstream of the reattachment shoulder were reduced by as much as a factor of three by mass injection within the cavity.

CONTENTS

INTRODUCTION . . . . .	1
EXPERIMENTAL DESIGN . . . . .	3
EXPERIMENTAL EQUIPMENT AND TECHNIQUES . . . . .	10
MEASUREMENTS OF PRESSURE DISTRIBUTION, MODEL A . . . . .	14
MEASUREMENTS OF PRESSURE DISTRIBUTION, MODEL B . . . . .	18
MEASUREMENTS OF HEAT TRANSFER RATE . . . . .	26
TOTAL-HEAD SURVEYS . . . . .	30
HOT-WIRE SURVEYS . . . . .	35
CONCLUDING REMARKS . . . . .	37
REFERENCES . . . . .	41

## LIST OF FIGURES

Figure	Page
1. Wind-tunnel Model geometry	42
2. Schlieren photograph of flow over basic cavity model at $p_o = 400$ psia, with $m_1 = \epsilon_g/L = 0$	43
3. Pressure distribution for $m_1 = \epsilon_g/L = 0$	44
4. Distribution of heat transfer coefficient for $m_1 = \epsilon_g/L = 0$	45
5. Photograph of mass-flow measurement plant from the front, with 3-inch helium hypersonic wind-tunnel in the background	46
6. Wind-tunnel models. From left to right, heat transfer model, pressure model B and pressure model A	47
7. Pressure distribution on model A, with $\epsilon_g/L = 0$	48
8. Effects of angle of attack on windward-side pressure distribution; model A with $\epsilon_g/L = 0$	49
9. Laminar similarity check	50
10. Comparison of pressure distributions measured by models A and B, with $\epsilon_g/L = 0$	51
11. Typical schlieren photographs of flow over model B with various values of $m_1$ and $\epsilon_g/L$	52
12. Measured pressure at mid-point of cavity floor, against $m_1$ and $\epsilon_g/L$	54
13. Pressure distribution on model B, $\epsilon_g/L = 0.016$	55
14. Pressure distribution on model B, $\epsilon_g/L = 0.032$	56
15. Pressure distribution on model B, $\epsilon_g/L = 0.048$ .	57
16. Pressure distribution on model B, $m_1 = 2$ $\mu$ slugs/second	58
17. Effect of mass injection on average heat transfer rate at cavity reattachment shoulder	59
18. Effect of mass injection on heat transfer rate at downstream station (1).	60
19. Effect of mass injection on heat transfer rate at downstream station (2)	61
20. Total-head surveys at station near reattachment shoulder, $\epsilon_g/L = 0.032$	62

21. Total-head surveys, downstream station, $\epsilon_g/L = 0.032$	63
22. Total-head surveys, far downstream station $\epsilon_g/L = 0.032$	64
23. Schlieren photographs of total-head probe traverses and interference studies	65
24. Oscilloscope traces obtained during hot-wire surveys of boundary layer downstream of R , with $m_1 = \mu\text{slugs/second}$ , and $\epsilon_g/L = 0.032$	66
25. Schlieren photographs of hot-wire traverses of boundary layer downstream of R , with $m_1 = 10 \mu\text{slugs/second}$ , and $\epsilon_g/L = 0.032$	67

## NOTATION

C	Viscosity-temperature proportionality constant
D	Cavity depth
h	Heat transfer coefficient
L	Length of cavity
$L_1$	Length of model from nose to separation point, for $\epsilon_s = 0$
M	Mid-point of cavity floor
$m_1$	Mass injection rate
p	Pressure
q	Local heat transfer rate
R	Cavity reattachment shoulder point
Re	Reynolds number
r	Radius of an axisymmetric model
S	Cavity separation shoulder point
T	Absolute temperature
u	Velocity component in direction parallel to basic cone surface
$\tilde{x}$	Wetted length along a generator of axisymmetric cavity model with origin at reattachment point. Positive sense downstream.
y	Coordinate measured normal to surface of basic cone
$y_1$	Height of dividing streamline above basic cone surface
$\beta$	Half-angle of basic cone
$\epsilon_s$	Height of separation shoulder above reattachment shoulder, measured perpendicular to basic cone surface
$\zeta_1$	Mass injection parameter used in Reference 1, and defined in the second section of the present report
$\mu$	Coefficient of viscosity
$\rho$	Mass density

### Subscripts:

cone	Properties on basic cone surface
floor	Properties on cavity floor
e	Properties at edge of boundary layer or shear layer
o	Isentropic stagnation conditions

PC Properties in plenum chamber  
R Reattachment shoulder point  
S Separation shoulder point  
T Stagnation conditions behind a normal shock  
w Conditions at the model wall

## INTRODUCTION

The present paper describes an experimental investigation of a hypersonic cavity flow with mass injection into the separated flow region. This work forms part of a continuing program of flow separation studies being carried out at the Gas Dynamics Laboratory of Princeton University. The investigation was based almost entirely on the work of References 1 and 2\*, and a brief summary of these two references will serve to introduce the present work.

The theoretical analysis of Chapman in Reference 1 was essentially a study of the laminar mixing layer set up when a compressible, high-velocity stream encounters a region of fluid at rest. By imposing a number of geometric restrictions, Chapman applied his solution of this free-mixing problem to a cavity flow in which separation took place with zero initial boundary layer thickness, and in which mixing occurred at substantially constant pressure. It was then shown that the integrated heat transfer rate to the wall of such a cavity was only 56% of that which would occur with a laminar attached boundary layer, this fraction varying slightly with the Prandtl number of the gas considered. In an extension of his theory to cavity flows with mass injection, Chapman showed that relatively small quantities of fluid injected into the separated region could reduce the wall heat transfer rate to zero.

The experimental investigation of Reference 2 consisted of measurements of the distributions of pressure, local recovery factor and local heat transfer coefficient in a matched set of laminar open cavity flows at hypersonic Mach numbers. No mass

---

\* A condensed version of Reference 2 is available in the open literature as Reference 3.

injection was employed. Several of the configurations studied simulated Chapman's theoretical flow model closely, and for these, integration of the local heat transfer coefficient yielded values of the overall heat transfer to the cavity surfaces which were in excellent agreement with the theory of Reference 1.

The conclusion that replacing a laminar boundary layer by a laminar cavity flow could reduce the heat transfer rate by almost a factor of two was of practical interest in obtaining local heat transfer protection for hypersonic flight vehicles. However, the work of Reference 2 showed that the cavity flow produced other, less desirable effects. In the vicinity of cavity reattachment, local heat transfer coefficients several times larger than the attached flow value were produced. These high heat transfer rates took almost one cavity length downstream of reattachment to decay to the attached flow value. When integration was extended to include the downstream surface as well as the cavity, it was found that the high heat transfer rates downstream of reattachment nullified almost all of the reduction obtained in the separated-flow region itself. It was therefore concluded in Reference 2 that in terms of reducing the overall heat transfer rate, the laminar cavity flow offered no net advantage, though it certainly provided a significant redistribution of local heat transfer rate.

The present work is an extension of the experiments of Reference 2 to include the effects of mass injection into the separated flow region. The investigation was partly motivated by the desire to check Chapman's prediction that mass injection has a powerful effect in reducing the overall heat transfer rate in a laminar cavity flow. It was hoped that mass injection might remove or reduce the high downstream heat transfer rates present in the basic cavity flow. More generally, the investigation

was intended as a pilot study to look into the possibilities of an extensive experimental investigation of various attached and separated flows with mass injection. Unlike the work of Reference 2, the present research is exploratory in nature. No attempt has been made to carry out an exhaustive study of a large number of flow configurations. Rather, the present work attempts to answer a number of specific questions about a particular type of cavity flow with mass injection and to set up an experimental framework within which further investigations might be initiated.

#### EXPERIMENTAL DESIGN

The basic model geometry chosen for the present experiments was identical to one of the configurations studied in Reference 2. The configuration consisted of an annular cavity of length-depth ratio 5 mounted on the surface of a 20° total-angle cone. The geometry is shown in Figure 1.

Only one geometric change was made in adapting the configuration of Reference 2 to the present mass-injection studies. The separation shoulder was raised above the basic cone surface by an amount  $\epsilon_s$ . Broadly speaking, this change provided clearance for the mass injected into the cavity to pass downstream. More rigorously, the geometric parameter  $\epsilon_s$  and the mass injection rate  $m_1$  were used in a complementary sense to control the pressure distribution over the model.

The parameters  $\epsilon_s$  and  $m_1$  were the only quantities varied throughout the present investigation. Apart from a few minor spot-checks, all other geometric and flow variables were held fixed. The investigation was carried out in the same test facility as had been used for Reference 2, namely the three-inch helium hypersonic tunnel of the Gas Dynamics Laboratory.

The geometric and fluid-dynamic variables held constant during the present study were as follows:

Wind-tunnel working fluid - helium

Injected gas - helium

$$Pr = 0.688$$

$$\gamma = 5/3$$

$$p_0 = 400 \text{ psia}$$

$$T_0 = 535^\circ R.$$

$$M_\infty = 11$$

$$\text{Angle of attack} = 0^\circ$$

All models axisymmetric

$$M_{\text{cone}} = 6.46$$

$$(Re_{e,S})_{\epsilon_S = 0} = 0.737 \times 10^6$$

Model nose diameter = 0.005 inches

$$L_1 = 1.25 \text{ inches}$$

$$L = 0.625 \text{ inches}$$

$$D = 0.125 \text{ inches}$$

$$L/D = 5$$

$$\beta = 10^\circ$$

$$0.82 \leq \frac{F}{F_0} \leq 1.08$$

In the above, the Reynolds number given is based on conditions at the edge of the boundary layer on a pure cone of  $20^\circ$  total-angle, and the characteristic length involved is  $L_1$ . This Reynolds number, and  $M_{\text{cone}}$  were calculated from Reference 4.

It should be noticed that the model wall temperature was always fairly close to the stagnation temperature of the stream. Such "hot-wall" conditions are typical of experiments in helium hypersonic tunnels, and the normal hypersonic complications of dissociation and ionization are deliberately avoided. In addition, the model nose diameter chosen was such that bluntness effects were not present, and the pressure on the basic cone surface was constant with axial distance from the nose (see Reference 2). As a result, the only "hypersonic" effect present in these experiments was the high Mach number.

With  $\epsilon_S = m_1 = 0$  the basic cavity flow described by the above list of variables was studied in detail in Reference 2. A summary of the data obtained under these conditions is given in the present report as Figures 2, 3 and 4. Figure 2 is a schlieren photograph showing the open cavity flow and the laminar boundary layers ahead of and behind the cavity. (Transition did not occur on the model at  $p_0 = 400$  psia.) Figure 3 gives the pressure distribution on the model. In this figure, the pressure at each point has been normalized by the pressure measured on a pure cone ( $\beta = 10^\circ$ ) at the same axial station. The abscissa is the wetted length along the model surface with origin at the cavity reattachment shoulder point (see Figure 1) normalized by the cavity length. The reattachment shoulder R and the mid-point of the cavity floor M have been indicated on the figure. The source of the data in Figure 3 was not only Reference 2 -- the other measurements will be discussed later. Figure 4 presents the distribution of local heat transfer coefficient on the cavity model, the data again being normalized by measured cone values. In this figure the separation point S is included within the range of the abscissa. The local recovery factor was found to be virtually constant

on this model under the above conditions. The mean value was about 0.81, which is close to the laminar attached boundary layer value for helium at these Mach numbers (see Reference 5).

The design of the present mass-injection experiments was strongly influenced by several features of the basic cavity flow. In Figure 4, it can be seen that even without mass injection, the heat transfer coefficient on the cavity floor is very low. The question of whether mass injection further reduces the floor heat transfer rate is of little practical importance. In order for mass injection to produce a significant effect on the overall heat transfer rate it is essential that the peak heat transfer rates in the vicinity of cavity reattachment be substantially reduced. Moreover, this local reduction must be achieved without increasing the heat transfer rates downstream of reattachment.

In view of the above considerations, attention was focussed throughout the present investigation on the region in the immediate vicinity of reattachment, and on the surfaces downstream of this region. The fear that mass injection within the cavity might produce unpleasant effects downstream of the reattachment shoulder was based on the form of the equation for conservation of energy within a control volume bounded by the cavity surfaces and the dividing streamline. Writing this equation in physical terms, we have

$$\begin{aligned} &\text{Heat transferred to wall} \\ &= (\text{shear and conducted energy crossing dividing streamline}) \\ &\quad + (\text{energy input from injected fluid}) \\ &\quad - (\text{energy which passes downstream} \\ &\quad \quad \text{over reattachment shoulder}) . \end{aligned}$$

The injected fluid thus provides a carrier layer which shunts the incoming energy downstream over the reattachment corner before it can be transferred to the cavity

surfaces. Since this fluid passes directly over the downstream surfaces, and contains any energy which has been prevented from reaching the cavity walls, we might expect the possibility of increased heat transfer rates in these downstream areas.

The choice of how mass should be injected into the cavity in the present experiments was made largely on the information available in Reference 1. For simplicity in this initial investigation the injected fluid was chosen to be helium gas, this being the wind-tunnel working fluid. Two criteria to be satisfied by the method of injection were suggested by Chapman's theoretical assumptions:

- (i) The mass should be injected with substantially zero momentum.
- (ii) The stagnation enthalpy of the injected fluid should be constant and equal to the enthalpy at the model wall temperature.

The obvious means of injecting fluid to satisfy the above requirements was to use a porous wall, but this was avoided in the present investigation partly because of misgivings about the uniformity of conventional sintered materials, and partly because the practical difficulties of working with these materials would have been a considerable inconvenience in an exploratory study. As a result, it was decided to use a large number of drilled holes on the floor of the cavity, leading to a plenum chamber inside the model.

To satisfy condition (ii) above, the plenum chamber temperature of the injection fluid was always held equal to the model wall temperature. It should be pointed out that this condition is not the most common restraint placed upon the total enthalpy of the injected fluid in studies such as the present work. In many investigations with attached flows, the injected gas is much colder than the wall itself, and the primary effect of such injection is to produce a significant reduction in recovery

factor in the steady state. We are more interested in suppressing the heat transfer coefficient in the present work, and Chapman's theory demonstrates that the condition  $T_{PC} = T_w$  leads to only a moderate reduction in recovery factor. The desirable result of both forms of suppression is, of course, a reduction in heat transfer rate.

The range of mass injection rate which should be investigated was chosen on the basis of Chapman's theory. The mass injection rate in Reference 1 is expressed in terms of a parameter  $-\zeta_1$ . The relation between  $m_1$  and  $-\zeta_1$  for an axisymmetric flow is given on page 34 of Reference 1. The present author believes that this equation has been misprinted, and that the correct version should be

$$-\zeta_1 = \frac{\sqrt{3} m_1}{2\pi r_R L \sqrt{\frac{\rho_e u_e \mu_e C}{L}}} \quad (1)$$

Evaluating Chapman's viscosity-temperature proportionality constant at a wall temperature  $T_w = T_0 = 535^\circ R.$ , and inserting the geometric and flow properties given previously for the present experiments into Eq (1), it can be calculated that

$$\zeta_1 = - 0.37 m_1 \quad (2)$$

where  $m_1$  is given in microslugs per second.

Chapman shows in Reference 1 that a value of  $-\zeta_1$  of 1.233 would be sufficient to reduce the wall heat transfer rate to zero in a laminar cavity flow. Inserting this value into Eq (2) yields a corresponding value of  $m_1$  of 3.33 microslugs/second.

The maximum mass flow rate studied in the present investigation was arbitrarily chosen to be three times Chapman's optimum value, or 10 microslugs/second. To get

some feel for this amount of mass injection in relative terms, 10 microslugs/second is about 40% of the mass flow contained in a laminar boundary layer on a pure cone at the axial station of the reattachment shoulder on the cavity models. (This boundary layer mass flow was calculated from Reference 5 to be about 26.6 microslugs/second in the present experiments.)

It was pointed out in the introduction to this report that the present investigation was not designed as an exhaustive study of a large number of flow configurations, but was intended to answer a number of specific questions about a particular cavity flow with mass injection. It will perhaps be useful to conclude this section by listing these questions:

- (i) Are the properties of a hypersonic cavity flow with mass injection sufficiently stable and well-defined to justify the initiation of a more general experimental program dealing with various mixing layers at very high Mach numbers?
- (ii) How can the effects of mass injection and separation shoulder height variation be combined to produce a desired pressure distribution in the cavity and downstream of reattachment?
- (iii) Are there particular combinations of  $\epsilon_S$  and  $m_i$  which will completely remove, or substantially reduce the high pressure peak found at reattachment in the basic cavity flow?
- (iv) Do small quantities of mass injection have a significant effect in reducing heat transfer rates in a hypersonic cavity flow, particularly in the critical reattachment region?
- (v) Does mass injection have an adverse effect on wall heat transfer rates downstream of the cavity reattachment shoulder?
- (vi) Do small quantities of mass injection have a drastic effect on the transition Reynolds number in a hypersonic cavity flow?

- (vii) Is Chapman's theory (Reference 1) sufficiently realistic to provide useful information on practical cavity flows with mass injection?

In the present report, an attempt is made to answer all of the above questions experimentally.

#### EXPERIMENTAL EQUIPMENT AND TECHNIQUES

In this section, only a brief description of the experimental techniques is given. A detailed description is available as Reference 6.

The wind-tunnel used for the experiments was the three-inch helium hypersonic tunnel of the Gas Dynamics Laboratory. This is a blow-down facility with a maximum running time of about ten minutes. A contoured nozzle was used for the present investigation, giving a uniform Mach number of eleven in the test-section. The wind-tunnel is fully described in Reference 7.

The mass-flow measurement plant used to supply helium to the injection plenum chambers of the wind-tunnel models was based on carefully calibrated sonic nozzles. The plant was designed to deliver between 0 and 10 microalugs/second of clean, dry and filtered helium gas to the models. An accuracy of about  $\pm 1\%$  in measuring the mass-injection flow rate was achieved in practice. The flow was monitored by manual control of the pressure in a large stagnation tank upstream of the choked nozzle. The measurement plant is shown from the front in Figure 5. The three-inch helium tunnel is in the background in this figure, with the stagnation chamber at the left and diffuser section at the right.

For the present investigation, two models were built to measure pressure distribution and one to measure heat transfer rates. The interior of each model

was used as a plenum chamber for the injected mass, and a pressure tap and thermocouple were incorporated in each chamber. Sixty-eight holes of 1/32 inch diameter were drilled in each cavity floor for mass injection.

The pressure models were built of brass, with copper leads to avoid outgassing effects. The two pressure models will be distinguished by the letters A and B in this report. Model A was a preliminary model, and had  $\epsilon_s = 0$ . This model incorporated rather sparse instrumentation on the cavity floor and downstream of the reattachment shoulder. Pressure model B incorporated detachable noses giving values of  $\epsilon_s$  of 0, 0.01, 0.02 and 0.03 inches. This model had much more complete instrumentation than model A, particularly in the immediate vicinity of the cavity reattachment shoulder.

The heat transfer model utilized the transient calorimeter technique, in which the temperature-time history of a known mass of material at the measuring station is studied. The model was primarily constructed of brass. The measuring elements were of copper, insulated by plexiglas supports. The temperature of each element was measured by copper-constantan thermocouples and fast-response self-balancing potentiometers. The wind-tunnel was fitted with a plug in the throat for heat transfer studies, and by quickly withdrawing this plug, the flow could be suddenly established over the model. High-speed motion pictures showed that even with mass injection, the final configuration of shock-waves and shear layers was established over the model in 2 milliseconds. The heat transfer model had detachable noses giving values of  $\epsilon_s$  of 0, 0.01 and 0.02 inches.

The heat transfer rate was measured at three stations: the immediate vicinity of the cavity reattachment shoulder, and at two stations downstream of the shoulder.

At the reattachment shoulder, the measuring element was a copper ring of approximately square cross-section, bounding the region  $-0.048 \leq \tilde{x}/L \leq 0.048$ . At station (1) downstream, the element was  $3/32$  inches in diameter and 0.02 inches deep, and was situated at  $\tilde{x} = 1/4$  inch. At station (2) the element was the same size, but was situated at  $\tilde{x} = 1/2$  inch.

All three wind-tunnel models incorporated four pressure taps spaced  $90^\circ$  apart at a single axial station downstream of the reattachment shoulder and these were used to align the models with the stream while the tunnel was running.

A photograph of the models is given in Figure 6. The mass-injection ports can be clearly seen, and the detachable noses are shown alongside the models.

By means of a simple traverse gear, the boundary layer downstream of the cavity reattachment shoulder was probed with a total head tube and a hot-wire. Because of physical limitations, the probes travelled along a line at  $35^\circ$  to the model surface rather than the more desirable  $90^\circ$ . This effect was not felt to be important for the qualitative studies required in the present instance.

Both probes were checked by traversing the laminar boundary layer on a pure  $20^\circ$  total-angle cone, and fairly severe limitations were observed on the data from both total-head tube and hot-wire. The total head tube was rectangular in section at the tip, with outside dimensions of 0.046 inches by 0.009 inches. This tube was large enough to cause measurable interference with the boundary layer, but qualitative data could still be obtained. The shortcomings of the total-head measurements will be discussed later. With the hot-wire, quite serious vibration problems were encountered, and in fact, a "turbulent" signal was obtained in the maximum  $\rho u$  gradient region of a boundary layer which was known to be laminar. This effect was believed to be caused by relative movement of the wire within the boundary layer,

resulting in a fluctuating signal. Only the most limited information was obtained from the hot-wire probe.

In the present report, the method of presenting the results is substantially the same as in Reference 2. Measurements of pressure or local heat transfer rate at a particular axial station on a cavity model have been normalized by the values of these quantities measured at the same axial station on a simple 20° total-angle cone. (Such a cone formed the basic geometry of all models studied in the present investigation.) The cone results used for this normalization may be found in Reference 2.

A particular axial station on a cavity model is characterized by the parameter  $\tilde{x}$  in this report. This distance is the wetted length along a generator of the model surface from the reattachment shoulder point, with the positive direction downstream (see Figure 1). All length parameters have been normalized by the cavity length  $L$  (5/8 inches).

The mass injection rate  $m_1$  has not been non-dimensionalized in the present work, but has simply been presented in microslugs/second. This course was followed because no single method of non-dimensionalization seems to have been accepted by experimentalists working in this field. Not enough work has been done with mass injection in separated flows for a particular non-dimensional parameter to have become standard. The parameter used by Chapman,  $\zeta_1$ , is geared to the requirements of his theory. It cannot be used to obtain a physical feel for the amount of mass injection, partly because  $\zeta_1$  includes a viscosity-temperature proportionality constant and partly because the injected mass is compared to a mass given roughly by that contained in an incompressible laminar boundary layer. A parameter

expressing the considerable growth in boundary layer thickness with increasing Mach number is not included. At any rate, the relation between  $\zeta_1$  and  $m_1$  given in microslugs/second has been given in Eq (2). Perhaps the best feel for the mass injection rates used in the present investigation can be obtained by remembering that the mass flow contained in a laminar attached boundary layer at the reattachment shoulder station is 26.6 microslugs/second under the present experimental conditions.

#### MEASUREMENTS OF PRESSURE DISTRIBUTION, MODEL A

The distributions of pressure on model A with mass injection rates of 0 to 10 microslugs/second are given in Figure 7. The pressure on the cavity floor is seen to rise progressively as the mass injection rate is increased. A slight pressure gradient is present on the floor when mass is injected, and this pressure gradient becomes more pronounced with increasing  $m_1$ . Some distortion of the floor pressure distribution due to the concentration of mass injection ports in the reattachment corner is evident at mass injection rates greater than 4 microslugs/second.

Downstream of reattachment, the pressure level falls with increasing  $m_1$ . Close to reattachment there is some evidence that the pressure becomes almost constant at values of  $m_1$  greater than 4 microslugs/second, at a value of  $p/p_{\text{cone}}$  of about 0.93.

A large number of repeat tests was run on model A, and it was found that the data given in Figure 7 were repeatable to a high order of accuracy. The pressure distributions were within about  $\pm 1\%$  experimental spread. Tests were made at values of  $m_1$  intermediate to those given in Figure 7, but these have been omitted for clarity of presentation. The variation of the pressure distribution with  $m_1$  was smooth and monotonic at each station on the model.

It can be seen from Figure 7 that a mass injection rate of 2 microslugs/second was required to produce cone pressure on the cavity floor. (The floor pressure on the cavity model with  $m_1 = \epsilon_S = 0$  is about 15% less than cone pressure, as has been discussed in Reference 2.)

The pressure in the model plenum chamber was found to rise linearly with  $m_1$ . The pressure ratio across the mass injection ports was always subcritical during the present experiments, the minimum value obtained being  $p_{\text{floor}}/p_{\text{PC}} = 0.51$  at  $m_1 = 10$  microslugs/second. (The critical pressure ratio for helium is 0.487.) From these measurements, therefore, it is believed that injection was always subsonic, though the sonic velocity was approached at the highest mass injection rates.

As mentioned in the previous section, alignment of the wind-tunnel models was carried out while the tunnel was running using four pressure taps spaced 90° apart at a single axial station on each model.

The sensitivity of this system for the present mass injection tests was checked by deliberately misaligning model A, and measuring the windward-side pressure distribution with no mass injection and with  $m_1 = 3$  microslugs/second. Two angles of misalignment were chosen which gave significant changes in the alignment-tap pressure levels. These angles were measured from schlieren pictures and were found to be 17 and 42 minutes. The data from the tests are given in Figure 8.

It is seen from this figure that the pressure distribution on the model is less sensitive to changes in angle of attack when mass injection is used. This is particularly true within the cavity -- at  $m_1 = 3$  microslugs/second virtually no change in the windward-side pressure distribution is detectable even when the differential pressure at the alignment taps is almost 25% of the mean.

Apparently, the injection of mass into the cavity allows additional freedom for the flow to adjust to the misalignment. With no mass injection, the dividing streamline is forced to close at the model reattachment shoulder. With mass injection, this streamline is less constrained, and fluid can pass to leeward and out of the cavity over the reattachment shoulder.

It was concluded from these results that the method of alignment was quite adequate for the mass injection experiments. The downstream pressure taps were used to align each model with  $m_1 = 0$ , and this setting was held constant for  $m_1 > 0$ . The data of Figure 8 demonstrate that the model is being aligned in its most sensitive condition when this procedure is followed.

The final tests run on model A investigated the effects of changes in tunnel stagnation pressure. These experiments led to a preliminary indication that the flow over the entire model was laminar, at least for moderate mass injection rates. This conclusion was based on the following reasoning.

It is fairly clear that the variation of the pressure distribution on a cavity model with mass injection must be governed by the values of non-dimensional parameters which give the amounts of mass, momentum and energy being injected, relative to some typical quantities in the shear layer. If mass is injected with a specific total enthalpy equal to the enthalpy at the wall and with substantially zero momentum, then the principal assumptions of Chapman's theory have been satisfied. This theory demonstrates that under these assumptions the flow is characterized by a single parameter  $\zeta_1$ , which involves the mass injection rate alone.

In the present experiments, therefore, we might expect that if the ratio of the injected mass to some characteristic shear layer mass flow were kept constant,

then the pressure distribution on the configuration would remain constant, provided no significant momentum distortion occurred. The mass flow in the shear layer may be characterized by the quantity

$$\rho_e u_e \cdot \frac{2\pi r_R}{\sqrt{3}} \left[ \frac{L_1 + L}{\sqrt{Re_{R,e}}} \right]$$

where the factor in square brackets accounts for the change of the shear layer thickness with Reynolds number in laminar flow. For a given model geometry, therefore, we might expect the pressure distribution to be governed by the ratio

$$\frac{m_1 \sqrt{Re_{R,e}}}{\rho_e u_e} \quad \text{or} \quad \frac{m_1}{\sqrt{\rho_e}} \sqrt{\frac{(L_1 + L)}{\mu_e u_e}}$$

In particular, if we vary only the stagnation pressure (affecting the density  $\rho_e$  directly), the governing parameter is given by  $m_1 / \sqrt{p_0}$ .

Accordingly, tests were run on model A varying both the stagnation pressure of the tunnel and the mass injection rate in such a way as to keep the quantity  $m_1 / \sqrt{p_0}$  virtually constant. The results are presented, with a large ordinate scale, in Figure 9. It is seen that the maximum spread in measured pressure at any station is  $\pm 2\%$  in the  $p_0$  range 300 to 600 psia. When similar tests were made at a stagnation pressure of 800 psia, it was found that the similarity rule began to break down, the pressure distribution in the cavity being lower than that given by Figure 9. This could not be due to increasing injected momentum, since this effect would increase the cavity floor pressure rather than decrease it. The most logical interpretation is that transition was occurring between  $p_0 = 600$  and 800 psia; this would increase

the mass flow in the shear layer and would require a corresponding increase in  $m_1$  to bring the floor pressure up to the value given by the laminar similarity parameter  $m_1/\sqrt{p_0}$ .

Any conclusions made from the above results are necessarily tentative, since the range of  $p_0$  and  $m_1$  investigated was not large and the applicability of a laminar similarity law is hardly a very sensitive indicator of natural transition. However, additional evidence that the flow over model A was laminar at low mass injection rates was obtained from the measurements of plenum chamber temperature. For small  $m_1$ , the temperature in the plenum chamber was controlled by the model wall temperature. At the conclusion of runs made on model A with low mass injection rates it was found that  $T_{PC}$  was very close to the adiabatic wall temperature for laminar flow with  $m_1 = 0$ , as measured in Reference 2.

#### MEASUREMENTS OF PRESSURE DISTRIBUTION, MODEL B

As described in the third section of this report, pressure model B was built with various nose sections giving a number of values of  $\epsilon_S$ . Pressure taps were concentrated in the reattachment region.

The first tests run with model B were carried out for  $\epsilon_S = 0$ , and were designed to check the overlap between models A and B. Data from both models for  $\epsilon_S = 0$  and  $m_1 = 0$  are given in Figure 3. (This figure also includes data from model A with only 20 mass injection ports, a configuration which was abandoned for reasons given in Reference 6.) Comparison of the pressure distributions measured by each model with  $\epsilon_S = 0$ , and  $m_1 = 1, 3$  and 6 microslugs/second is given in Figure 10. At  $m_1 = 1$  and 3 microslugs/second, the distributions of pressure

outside the immediate vicinity of reattachment are seen to be virtually identical for the two models. However, at 6 microslugs/second and above, differences were observed in the reattachment corner. These errors are believed to be due to the strong jets formed at higher mass injection rates as the injection velocity increases. With such jets, the pressure measured at a particular tap probably depends on the tap position relative to the positions of the mass injection ports. It is apparent that the data from model B close to reattachment are unreliable above a mass injection rate of about 5 microslugs/second. Accordingly, no results from this model above  $m_1 = 5$  microslugs/second will be presented in what follows.

A physical picture of the flow configuration on model B may be obtained from the typical schlieren photographs given in Figure 11. These photographs show the flow for  $\epsilon_S/L$  values between 0 and 0.048, and with various values of  $m_1$ . At the highest values of mass injection rate, the schlieren pictures show some indication of transition at the rear of the model (well downstream of reattachment), but otherwise the shear and boundary layers look laminar throughout.

Examination of the schlieren pictures of Figure 11 shows that, in general, the angles turned by the flow at the separation point are quite small for the range of  $m_1$  and  $\epsilon_S$  investigated in the present experiments. In fact, only at  $\epsilon_S = 0$ ,  $m_1 = 10$  microslugs/second is the distortion of the flow sufficient to cause noticeable interference with the bow-wave. In addition, it can be seen from the schlieren photographs of Figure 11 that the white line representing the outer part of the shear layer is virtually straight in the front part of the cavity. In the light of these observations, it might be anticipated that the pressure on the forward part of the cavity floor would be almost constant, at least for the moderate range

of  $m_1$  and  $\epsilon_g/L$  investigated with model B . In fact, we have already seen that this is true for  $\epsilon_g/L = 0$  (Figures 7 and 10). Results will be presented later which will show that an almost constant pressure over the front part of the cavity floor was obtained for all values of  $m_1$  and  $\epsilon_g/L$  investigated with model B.

The value of cavity floor pressure which occurs in a particular configuration will, of course, depend on the values of each of the parameters  $m_1$  and  $\epsilon_g/L$  . For the small angles we are presently considering, it is reasonable to expect that the cavity floor pressure will be determined by the angle between the dividing streamline in the upstream part of the cavity and the basic cone surface. This cannot be strictly true, since for one thing, we are neglecting the displacement effect of that part of the viscous layer outside the dividing streamline. In addition, we have no conclusive evidence that the pressure at the dividing streamline is the same as that on the wall beneath it ( ie  $\frac{\partial p}{\partial y} = 0$  ) . However, the assumption is probably quite good, and it allows some clarification of the processes which determine the floor pressure.

Let us first consider the effects on the angle between the dividing streamline and the cone surface of each of the parameters  $\epsilon_g/L$  and  $m_1$  acting alone. With  $m_1 = 0$  , the dividing streamline must reattach to the model surface. For values of  $\epsilon_g/L$  up to about 0.04, it was shown in Reference 2 that reattachment occurs very close to the model reattachment shoulder, R . At higher values of  $\epsilon_g/L$  , reattachment begins to move downstream of R , leading to a flow more typical of that over a rearward-facing step than a true cavity flow. If the dividing streamline is almost straight, then the angle it makes with the cone surface will be about equal to  $\epsilon_g/L$  , at least before reattachment moves downstream. Indeed, it was demonstrated in

Reference 2 that the cavity floor pressure for  $m_1 = 0$  was given quite closely by the first term of a Prandtl-Meyer flow using  $\epsilon_S/L$  as the turning angle, for values of  $\epsilon_S/L$  below 0.04.

With  $\epsilon_S/L = 0$ , the height of the dividing streamline above the cone surface at the shoulder point R is given by

$$y_1 = \frac{m_1}{2\pi r_R \int_0^1 \rho u d\left(\frac{y}{y_1}\right)} \quad (3)$$

If the dividing streamline were virtually straight, then the angle made by this streamline with the cone surface would be given approximately by  $y_1/L$ . Using Eq (3) and our previous assumptions, the floor pressure increment due to  $m_1$  alone would be roughly proportional to

$$\frac{m_1}{2\pi r_R L \int_0^1 \rho u d\left(\frac{y}{y_1}\right)}$$

The integral in the denominator of this expression depends on  $m_1$ , and a knowledge of the nature of this dependence could come only from a full analysis of the mixing problem being considered. However, in the light of the possibility that the integral expression is a slowly-varying function of  $m_1$ , it would be logical to look for a floor pressure increment almost directly proportional to  $m_1$  as given by the numerator of the above expression.

The dependence of the cavity floor pressure on  $m_1$  and  $\epsilon_S/L$  was determined experimentally in the present investigation using model B. Figure 12 gives the measured pressure at the mid-point of the cavity floor for a moderate range of both  $m_1$  and  $\epsilon_S/L$ . Figure 12 is a form of three-dimensional graph known as a "carpet plot". Each unit of the abscissa represents 1 microslug/second in  $m_1$  or 0.016 in  $\epsilon_S/L$ . The experimental values of  $P_{\text{floor}}/P_{\text{cone}}$  for  $\epsilon_S/L = 0$  are first plotted against  $m_1$  with an arbitrary origin. To plot the data for  $\epsilon_S/L = 0.016$ , the origin of  $m_1$  is moved one unit to the right. The process is repeated for the other values of  $\epsilon_S/L$ . Experimental points taken either at the same value of  $m_1$  or at the same value of  $\epsilon_S/L$  have been connected by straight lines in Figure 12. The resultant network of lines is therefore built up from isolines of  $m_1$  and isolines of  $\epsilon_S/L$ .

It was observed in the preceding discussion that the floor pressure increment due to  $\epsilon_S/L$  alone would be expected to be directly proportional to  $\epsilon_S/L$  for a limited range of this parameter. In addition, the possibility existed that the floor pressure increment due to  $m_1$  alone might be roughly proportional to  $m_1$ . If these variations were strictly correct, and if the effects of  $\epsilon_S/L$  and  $m_1$  were completely independent of one another, then the network of Figure 12 would consist of two sets of straight parallel lines. Examination of the figure will show that such a network would be a very good approximation to the experimental results.

It is clear from Figure 12 that within the test rhombus there is an infinite number of combinations of  $m_1$  and  $\epsilon_S/L$  which will produce a particular desired floor pressure. The limits on the floor pressure which can be achieved are given by the two isolines  $m_1 = 0$  and  $\epsilon_S/L = 0$ .

Besides these floor pressure measurements, model B was used to obtain complete pressure distributions for various values of  $m_1$  and  $\epsilon_g/L$ , particularly in the region close to the model reattachment shoulder. Figure 10 contains some of the data for  $\epsilon_g/L = 0$ . Typical pressure distributions measured with values of  $\epsilon_g/L$  of 0.016, 0.032 and 0.048 are given in Figures 13, 14 and 15, respectively.

With zero mass injection, the data in Figures 13, 14 and 15 show that the pressure peak at reattachment is reduced as  $\epsilon_g/L$  increases. For  $\epsilon_g/L = 0.048$  (Figure 15), the peak has disappeared entirely and has been replaced by a monotonic rise in pressure through the reattachment region. This pressure distribution is typical of the flow over a rearward-facing step, and the eventual transition to this type of flow at high values of  $\epsilon_g/L$  has been mentioned previously. For  $m_1 = 0$  in Figures 13, 14 and 15, it is apparent that cone pressure is re-established on the model by about one cavity length downstream of reattachment.

The pressure distributions for various finite mass injection rates in Figures 13, 14 and 15 are qualitatively similar to the data for  $\epsilon_g/L = 0$  in Figure 10. Taking the results for  $\epsilon_g/L = 0.032$  in Figure 14 as an example, it is seen that the floor pressure reaches the basic cone value when  $m_1 = 4$  microslugs/second. At this value of mass injection rate, the pressure downstream of the reattachment shoulder R is about 15% less than cone pressure. The two pressure levels are connected by a rather abrupt expansion region near the reattachment shoulder. This step-like behavior in pressure distribution is also present at  $m_1 = 3$  microslugs/second, though the pressure levels on the cavity floor and downstream of R are closer together. However, at  $m_1 = 2$  microslugs/second, the pressure levels upstream and downstream of R are about equal, and the only distortion in the distribution

at R is a slight bump of about 5% of the cone pressure. At this mass injection rate, the pressure rises quite gently from a value of  $0.825 p_{\text{cone}}$  at the middle of the cavity floor to about  $0.92 p_{\text{cone}}$  one cavity length downstream of the reattachment shoulder

It would appear from the results of Figures 13, 14 and 15 that for each value of  $\epsilon_g/L$  a mass injection rate can be chosen which will produce an almost constant pressure distribution within and downstream of the cavity, with minimal disturbance at the reattachment shoulder. It is rather surprising to notice that for each value of  $\epsilon_g/L$ , the "optimum" value of  $m_1$  is about the same, namely 2 microslugs/second. (No attempt was made to seek slight improvements by varying  $m_1$  around 2 microslugs/second.) This behavior is shown more clearly in Figure 16, which shows the pressure distribution on model B with  $m_1 = 2$  microslugs/second for each value of  $\epsilon_g/L$  tested.

Figure 16 shows that  $\epsilon_g/L$  has a strong effect on floor pressure level, and this fact was noted previously in discussing the data of Figure 12. However, the effect of  $\epsilon_g/L$  diminishes downstream, and has almost disappeared one cavity length downstream of the model shoulder point, R. In addition, the strong qualitative similarity between the four distributions in Figure 16 would indicate that the shape of the pressure distribution near the shoulder R and downstream is controlled primarily by the mass injection rate alone.

It is possible that the controlling effect of the mass injection rate on the pressure distribution near and downstream of R is a result of the constraint imposed on the dividing streamline when it nears the model surface. In a cavity flow without mass injection, the dividing streamline necessarily reattaches to

the model surface. When mass is injected into the cavity, the dividing streamline never reattaches, but is displaced from the downstream wall by an amount sufficient to pass the injected fluid. All of the injected mass must pass between the dividing streamline and the solid model wall. In the present instance, the shape of the dividing streamline downstream of  $R$ ,  $y_1(\tilde{x})$ , is given by

$$y_1(\tilde{x}) = \frac{m_1}{2\pi r(\tilde{x}) \int_0^1 \rho u d\left(\frac{y}{y_1}\right)} \quad (4)$$

The pressure distribution should be controlled by the slope of the dividing streamline, given by differentiating Eq (4) with respect to  $\tilde{x}$ . For a fixed value of  $m_1$ , any variations in the shape of the dividing streamline for  $\tilde{x} \geq 0$  can arise only through the dependence of the integral term in the denominator of the right hand side of Eq (4) on  $\epsilon_g/L$ . It would appear from the data of Figures 13, 14, 15 and 16, and indeed from the discussion concerning the data of Figure 12, that this dependence is not strong.

The fact that fixing the mass injection rate appears to exert a controlling influence on the shape and position of the dividing streamline near the reattachment shoulder may have a bearing on the rather sudden change in pressure level at  $R$  for values of  $m_1$  higher than the optimum. Within the cavity itself, the dividing streamline is free to bend outwards under the influence of the injected mass, but as soon as the shoulder is reached the flow must adjust itself to satisfy the requirements of Eq.(4).

It should be observed at this point that the present author is unaware of any theoretical analysis which could be used to evaluate the integral of Eq (4) and

thereby put the above physical arguments on a firm theoretical basis. The theory of Chapman in Reference 1 deliberately excludes the reattachment shoulder region from the analysis. If this fact were ignored and the mixing layer profiles of Chapman were blindly substituted into Eq (4), the dividing streamline would be found to be an infinite distance above the wall with a mass injection rate of only 3.33 microslugs/second.

#### MEASUREMENTS OF HEAT TRANSFER RATE

For reasons discussed in the second section of this report, the heat transfer model was designed to measure the heat transfer rate at three stations -- namely, in the immediate vicinity of the reattachment shoulder, and at two stations downstream of this region. Measurements made at the downstream stations can be considered local measurements, but for structural reasons, the measuring element at the reattachment shoulder measured the average heat transfer rate in a small region given by

$0.048 \leq \frac{\bar{x}}{L} \leq 0.048$  . Most of the results were obtained for a uniform wall temperature of 535°R., which was the stagnation temperature of the tunnel. For these measurements, the injected mass had a stagnation temperature of 535°R., as measured in the model plenum chamber.

The heat transfer measurements made at the reattachment shoulder are plotted as  $q/q_{\text{cone}}$  against mass injection rate in Figure 17. Data for values of  $\epsilon_g/L$  of 0, 0.016 and 0.032 are presented. It is immediately obvious from Figure 17 that mass injection drastically reduces the peak heat transfer rate in the critical reattachment shoulder region. The mass injection rates employed in these tests were quite modest -- the maximum value of 10 microslugs/second is less than half of the

mass flow in a laminar boundary layer at this station. Nevertheless, the heat transfer rate at the reattachment shoulder is seen to be reduced by as much as a factor of six with these mass flow rates.

Perhaps the most important point is that substantial reductions in heat transfer rate are obtained with mass injection rates which produce useful pressure distributions over the model. We have seen in the preceding section that a mass flow rate of 2 or 3 microslugs/second produces a pressure distribution which is almost constant over the model, with minimal disturbance near the reattachment shoulder. This mass flow rate is an order of magnitude less than that contained in a laminar attached boundary layer at the reattachment shoulder station, and is nevertheless capable of producing almost a threefold reduction in heat transfer rate near the shoulder.

Figure 17 shows that increasing  $\epsilon_S/L$  also decreases the heat transfer rates. It is difficult to compare the heat transfer reductions obtained with  $m_1$  and with  $\epsilon_S/L$  quantitatively since the two parameters are physically different. However, if an equivalence between a value of  $m_1$  and a value of  $\epsilon_S/L$  is defined on a basis of equal distortions of floor pressure level (see Figure 12), then the effect of  $m_1$  in reducing the heat transfer rate is considerably more powerful than the effect of  $\epsilon_S/L$ .

The experimental measurements of heat transfer rate at the two stations downstream of R are given in Figures 18 and 19, for  $\tilde{x}/L = 0.4$  and 0.8, respectively. Again, data have been presented for three values of  $\epsilon_S/L$ , and for mass injection rates up to 10 microslugs/second. These results show that mass injection strongly reduces the downstream heat transfer rates, at least within one cavity length from the reattachment shoulder. For  $m_1 = 5$  microslugs/second the reduction is about a factor of two. Increasing  $\epsilon_S/L$  again appears to reduce the

heat transfer rates, but for these downstream stations the experimental inaccuracy allows a less positive conclusion.

It is clear from the results in Figures 18 and 19 that the fears expressed in the second section concerning the downstream heat transfer rates are unfounded -- mass injection within the cavity does not cause increased heat transfer rates downstream. In fact, substantial reductions in heat transfer are obtained over the entire region of interest in the present configuration.

The results given in Figures 17, 18 and 19 are measurements of heat transfer rate only, and we have described the results obtained for  $T_w = T_o = 535^\circ R.$ , in which heat transfer is from the model to the stream. In aerodynamic configurations of practical interest, we are concerned with heat transfer from stream to body, namely, the "cold-wall" case. To properly apply hot-wall results such as the present studies to practical aerodynamic cases, we would really require measurements of the heat-transfer coefficient, together with measurements of the recovery factor. Even then, it would be necessary to be sure that the modified Newtonian law (independence of heat transfer coefficient and wall temperature) held throughout the range of wall temperature considered. In the present investigation, measurements of recovery factor were beyond the reach of the techniques developed in Reference 2, because of the feedback between model wall temperature and plenum chamber temperature. To measure the adiabatic wall temperature, it would have been necessary to allow the model to reach equilibrium temperature in the tunnel while adjusting the plenum chamber temperature to be equal to the temperature of the outside wall. At higher mass injection rates, this would have required pre-cooling of the injected gas, and in any case, the adjustment process would have taken longer than the tunnel running time.

In a minor attempt to obtain some information on the generality of the present heat transfer measurements, a few tests were run at a wall temperature of 576°R. The model was raised to this wall temperature by using infra-red heat lamps. It was found that a mass injection rate as high as 3 microslugs/second could be used before the plenum chamber temperature fell too far below the model wall temperature. (A difference between  $T_{PC}$  and  $T_w$  of 5°R. was considered tolerable.) The heat lamps were switched off shortly before the flow was started over the model. These tests were run for  $\epsilon_g/L = 0.032$ , and the results are given as the solid symbols in Figures 17, 18 and 19. The data points fall quite close to the line for  $T_w = 535^\circ R.$  and  $\epsilon_g/L = 0.032$ , and it can be inferred that the results given for  $q/q_{cone}$  are probably indicative of the variation of  $h/h_{cone}$  with  $m_1$  in this wall temperature range.

The present measurements of heat transfer rate with the calorimeter technique should be quite accurate in a relative sense, but the absolute values will not be so accurate as measurements made using the "thin-wall" technique. This is because the measuring elements must be weighed before thermocouple wires are attached, and the solder used for the latter purpose inevitably adds an unknown mass at each element. However, we can obtain an idea of the absolute accuracy by comparing the present results for  $m_1 = \epsilon_g/L = 0$  with the measurements made on this cavity configuration in Reference 2.

The calorimeter technique was used to measure the average heat transfer rate in the immediate vicinity of the reattachment shoulder in Reference 2 and the measuring element was ostensibly the same size as that used for the present experiments. However, the present element appears to have been machined slightly

larger than that used in Reference 2, since for  $m_1 = \epsilon_S/L = 0$  a value of  $q/q_{\text{cone}}$  of 2.21 was obtained in the present work as compared to a value of  $q/q_{\text{cone}}$  of about 2.4 in Reference 2. ( $h/h_{\text{cone}}$  was 2.63 in Reference 2 but the recovery factor on a cavity flow without mass injection is slightly higher at reattachment than elsewhere.) The downstream heat transfer results for  $m_1 = \epsilon_S/L = 0$  are compared with the measurements made using the thin-wall technique in Reference 2 in the following table.

<u>Downstream station</u>	<u><math>q/q_{\text{cone}}</math>, present work</u>	<u><math>h/h_{\text{cone}}</math>, Reference 2</u>
(1)	0.93	1.11
(2)	0.91	0.93

The absolute accuracy of the present results is seen to be quite good for station (2), but poor for station (1). However, our main interest in the present investigation is in relative heat transfer measurements obtained with various amounts of mass injection.

#### TOTAL-HEAD SURVEYS

The measurements made in the present investigation with the forward-facing total-head tube were designed to obtain qualitative information on the development of the boundary layer downstream of the reattachment shoulder. Traverses of this layer were made for a value of  $\epsilon_S/L$  of 0.032, at mass injection rates of 0, 4, and 10 microslugs/second. Three survey stations were chosen: one in the immediate vicinity of  $R$ , one about midway between  $R$  and the end of the conical section of the model, and one far downstream near the end of the conical section. As mentioned in the third part of this report, traverses were not made perpendicular to the model

surface, but at an angle of about  $35^\circ$  to it. The experimental data are given in Figures 20, 21 and 22. In these figures the ordinate is the distance perpendicular to the wall in cavity lengths, and the abscissa is the pressure measured at the tube normalized by the tunnel stagnation pressure. In each figure a scale drawing of the traverse line in relation to the model geometry is given.

Figure 20 shows the results of a traverse made close to the reattachment shoulder. The cavity was not entered in these surveys, and  $y/L$  was always greater than zero. The most striking feature of the data in Figure 20 is the thick subsonic zone present at  $m_1 = 4$  and 10 microslugs/second. The value of  $p_T/p_0$  corresponding to sonic velocity in these tests was between about 1.1 and  $2 \times 10^{-3}$  depending on the model pressure distribution at the traverse station and the values of  $m_1$  and  $\epsilon_S/L$  being studied. (Taking the static pressure ahead of the probe as cone pressure gives a value of  $p_T/p_0$  of  $1.4 \times 10^{-3}$  for sonic velocity.) In Figure 20, the subsonic layer at  $m_1 = 10$  microslugs/second occupies almost half the shear layer thickness.

Examination of the data of Figure 20 indicates that, roughly speaking, the effect of mass injection within the cavity is to push the shear layer away from the model surface. The curves in Figure 20 show that little mixing has taken place by the time the reattachment shoulder is reached. The presence of the deep subsonic zone with  $m_1 = 4$  and 10 microslugs/second makes it easier to understand the pronounced effect of mass injection on wall heat transfer near the reattachment shoulder.

Results from traverses made some distance downstream of R are given in Figure 21. Comparison of this figure with Figure 20 shows that considerable mixing has taken place by the time this station is reached. The peak in  $p_T/p_0$  at the edge

of the boundary layer in each traverse is believed to be due to slight boundary layer separation resulting from the normal shockwave in front of the probe, and this interference effect has been mentioned in the third section of the present report.

It is suggested that the shockwave from the probe interacts with the boundary layer, thickening it slightly ahead of the probe. This would produce compression waves to allow a more efficient compression of the flow reaching the probe. The result would be an indication of higher values of  $p_T/p_0$  than actually exist. Evidence from schlieren photographs and cone boundary layer traverses in support of this explanation is available in Reference 6.

Comparing the data of Figure 21 with those of Figure 20 it can be seen that, as expected, the thickness of the boundary layer for  $m_1 = 0$  is greater at the downstream station than at the upstream station. However, with mass injection rates of 4 and 10 microslugs/second, the boundary layer thickness appears rather smaller downstream than near the reattachment shoulder. Going even further downstream, the data of Figure 22 show that the boundary layer thicknesses with mass injection are about the same as those measured in Figure 21, in contrast to the data for  $m_1 = 0$ . This behavior is believed to be due to the fact that there are two conflicting factors affecting the boundary layer growth downstream of  $R$ , when mass injection is used. One of these factors is the viscous effect, which will act to increase the boundary layer thickness. The other effect is the decreasing thickness of the layer bounded by the model surface and the dividing streamline with finite mass injection. Equation (4) shows that the dividing streamline approaches the wall downstream because of the  $1/r$  term resulting from the present conical configuration. (We are assuming that this effect is not smothered by any decrease in the integral

term in Eq (4) with increasing  $\tilde{x}$ .) It is suggested that these two effects are almost balanced in the present configuration. Additional evidence for the virtually constant boundary layer thickness downstream of R is available in the schlieren photographs of Figure 11.

The results of Figure 22 for the far downstream station show that mixing has progressed still further by this station. The results of the traverse made at  $m_1 = 10$  microslugs/second are interesting. In contrast to the results at the other stations, this particular curve is not virtually parallel to the curves for  $m_1 = 0$  and  $m_1 = 4$  microslugs/second in the maximum-shear region; close to the wall the curve crosses that for  $m_1 = 4$  microslugs/second, and the curve does not contain the peak at the edge of the shear layer exhibited by the other traverses. It is believed that these differences in this particular traverse were due to the boundary layer being transitional at  $m_1 = 10$  microslugs/second for this downstream station. Evidence will be presented from hot-wire studies in the next section to support this contention. The absence of the peak at the edge of the shear layer for  $m_1 = 10$  microslugs/second in Figure 22 is felt to be due to the fact that separation occupies a much smaller region in a transitional or turbulent layer than in laminar flow, and the transitional layer is much better able to withstand the probe interference effect described previously.

In the traverses made at the downstream stations sufficient measurements were made for the probe to indicate the total-head level outside the boundary layer, as given by the asymptotic value of  $p_T/p_0$  for large  $y/L$ . When these asymptotic levels were converted to Mach numbers, assuming that the static pressure ahead of the probe was equal to the pressure measured at the model wall, the values obtained

for the six curves in Figures 21 and 22 ranged between 6.37 and 6.62. The theoretical Mach number at the edge of the pure cone boundary layer under the present experimental conditions is 6.46. It is apparent that the present configurations conform to the conventional supersonic continuum-flow picture of a clearly defined boundary layer and an isentropic outer flow, despite the hypersonic Mach numbers and thick viscous layers encountered in the present studies.

The first two photographs in Figure 23 are typical schlierens of the probe traverses at  $m_1 = 10$  microslugs/second. In the first photograph, the probe is close to the model wall at the middle traverse station and is immersed in a laminar boundary layer. In the second schlieren, the probe is immersed in what is believed to be a transitional layer at the traverse station furthest downstream.

Because of the thickness of the subsonic zone with mass injection, there was some concern that the shoulder on the model where the conical section joined the cylindrical support might influence the model surfaces upstream. This was checked by introducing various disturbances near the shoulder and monitoring the pressure distribution on the model. No disturbance was ever found upstream of about one cavity length downstream of  $R$ . A typical schlieren picture of the model with  $\epsilon_S/L = 0.032$ ,  $m_1 = 4$  microslugs/second and with disturbance elements near the shoulder is given as the last picture in Figure 23. In retrospect, it is not surprising that no upstream influence was found. The subsonic zone is very thick near the reattachment shoulder for high mass injection rates, but the mixing downstream reduces the thickness of the zone quite quickly.

### HOT-WIRE SURVEYS

In the third section of the present report, the serious limitations of the hot-wire equipment used in this investigation were mentioned. The occurrence of an unsteady signal in the outer half of a boundary layer which was known to be laminar was noted. In fact, the only ways in which the present hot-wire equipment appeared capable of distinguishing a turbulent boundary layer were in the narrowness of the laminar signal zone near the wall and in the slowness with which the turbulent signal died off as the hot-wire was moved into the external stream.

Hot-wire surveys were made of the boundary layer downstream of the reattachment shoulder at the same three axial stations as had been used for the total-head studies. Again, mass flow rates of 0, 4 and 10 microslugs/second were used.

In all of the traverses except one the hot-wire results indicated laminar flow -- in other words, the signals obtained at various positions in the boundary layer were qualitatively identical to those obtained when studying the laminar boundary layer on a pure cone. The three oscilloscope traces shown at the left in Figure 24 are typical of the results obtained in a flow believed to be laminar. These photographs were taken on a traverse near the reattachment shoulder with a mass injection rate of 10 microslugs/second. The positions of the hot-wire when each of these oscilloscope traces was recorded are given in the schlieren photographs of the first half of Figure 25.

The first oscilloscope trace in Figure 24a shows a laminar signal (ie one indistinguishable from the noise level in the circuit) and was taken just at the edge of the boundary layer (Figure 25a). The second trace, Figure 24b, was taken when the hot-wire was moved a few thousandths of an inch into the boundary layer

(Figure 25b) and shows the sudden change to a significantly unsteady signal. This type of signal was obtained in the maximum-shear section of the laminar boundary layer on a pure cone. ("Maximum-shear" is used here to denote the region of strong gradient in  $\rho u$ .) The third photograph, Figure 24c, again shows a laminar signal, and was taken with the hot-wire still a significant distance from the wall (Figure 25c). The important point is that the zone of unsteady signal is extremely thin when the boundary layer is laminar.

The three oscilloscope photographs to the right of Figure 24 were also taken with  $m_1 = 10$  microslugs/second, but in this case the traverse was made near the end of the conical section of the model. In this case, the boundary layer appeared to be turbulent, or at least transitional. This was the only turbulent traverse encountered during these hot-wire studies. The first trace, in Figure 24d is not laminar and yet this trace was taken quite close to the wall (see Figure 25d). The second trace is unsteady, and this was taken in the maximum-shear zone (Figures 24e and 25e). The third trace was taken some distance out into the external stream, and does not show a laminar signal (Figure 24f). The hot-wire position can just be seen in Figure 25f. The "turbulent" signal in this last oscilloscope photograph may be due to turbulent fluctuations or to wave radiation from the turbulent layer. To summarize, on this particular traverse it was difficult to obtain a laminar signal anywhere, even very close to the wall or well out towards the bow-wave.

Attempting to obtain a quantitative estimate of the transition Reynolds number from these rather crude results is a little presumptuous, but if transition is taken as beginning half-way between the reattachment shoulder R and the end

of the conical section at  $m_1 = 10$  microslugs/second, this would give a transition Reynolds number of about  $1.4 \times 10^6$ . This may be compared with the transition Reynolds number for this cavity flow without mass injection, which is about  $2 \times 10^6$  (see Reference 2. The transition Reynolds number given is again defined for the beginning of transition.) However, it must be remembered that transition was only observed at the maximum mass flow rate, and this mass flow rate was sufficient to cause some momentum-distortion of the pressure distribution. The present geometry is hardly suitable for injection rates as high as this. In any case, transition did not appear until the farthest downstream traverse station was surveyed.

Attempts were made to make hot-wire surveys at stagnation pressure levels higher than 400 psia, since it was known that at 1000 psia, transitional flow could be obtained even on a pure cone. However, the wires used would not even survive in the free stream, let alone traverse the bow-wave.

#### CONCLUDING REMARKS

In this section, the conclusions drawn from the present exploratory investigation into the effects of mass injection in a laminar, hypersonic cavity flow are given. In form and sequence, these conclusions will be given as answers to the questions listed in the second section of the present report.

The flow regime studied was found to be stable, well-behaved and predictable throughout the range of mass injection rate and separation shoulder height investigated. The flow field appeared from optical studies to be steady, and all measurements made were always repeatable to an acceptable accuracy.

(As good as  $\pm 1\%$  in the measurement of pressure distribution, for example.)

The present exploratory study gives every indication that an extensive investigation of various mixing layers at these high Mach numbers would be worthwhile.

To summarize the observed effects of  $m_1$  and  $\epsilon_S/L$  on the pressure distributions over the cavity models we may conveniently divide the configuration into three regions. Over the upstream two-thirds of the cavity floor, the pressure was found to be virtually constant for all values of  $m_1$  and  $\epsilon_S/L$  studied. In this region, the floor pressure was strongly dependent on both  $m_1$  and  $\epsilon_S/L$ , the effects of these two variables being virtually independent. Increasing the mass injection rate produced an increase in floor pressure which was almost directly proportional to the change in  $m_1$ . Increasing the height of the separation shoulder relative to the height of the reattachment shoulder produced a decrease in floor pressure which was almost directly proportional to the change in  $\epsilon_S/L$ .

In the region a short distance downstream of the reattachment shoulder  $R$  ( $\tilde{x}/L$  greater than about 0.2) the pressure varied rather slowly. Far downstream of the shoulder, the pressure would presumably tend asymptotically to the basic cone value, but the models studied were not long enough to investigate this trend further than one cavity length downstream of  $R$ . The pressure level obtained on the downstream surfaces in the region  $0.2 \leq x/L \leq 1.0$  depended on both  $m_1$  and  $\epsilon_S/L$ , falling rather slowly with increases in either parameter.

In the third region, the vicinity of the reattachment shoulder, adjustment took place between the pressure levels in the other two regions. This matching region usually took the form of a simple step in pressure distribution, with a rather abrupt compression or expansion near the reattachment shoulder.

In most cases, the step was preceded by a rise to some peak pressure higher than the floor pressure. The shape of the pressure distribution in this matching region was governed almost entirely by the mass injection rate alone. Only for the smallest values of  $m_1$  (less than 2 microslugs per second) was there any significant effect of  $\epsilon_S/L$ .

It was found that for an "optimum" mass injection rate a pressure distribution could be obtained which exhibited minimal disturbance in the matching region. For this optimal  $m_1$ , the pressure levels in the upstream and downstream zones were roughly equal, and the pressure peak at the reattachment shoulder was very small. The optimum value of  $m_1$  was apparently virtually independent of  $\epsilon_S/L$ .

The relatively small quantities of mass injection used in the present investigation had a pronounced effect in reducing the heat transfer rates in the vicinity of the cavity reattachment shoulder. Injection of an amount of mass flow of about 2 to 3 microslugs/second (roughly the "optimum" value mentioned above) reduced the heat transfer rates near the shoulder by the factor of three. This quantity of mass injection is about one-tenth of that contained in a laminar attached boundary layer at the reattachment shoulder station. Increasing  $\epsilon_S/L$  also lowered the heat transfer rates at the reattachment shoulder, but the effect was not so powerful as that of mass injection.

The heat transfer rates downstream of the cavity reattachment shoulder were substantially reduced by injecting mass into the cavity, at least for the region within about one cavity length downstream of the shoulder.

Evidence on whether the flow over the cavity models with mass injection was laminar or turbulent was obtained from a number of sources. These included:

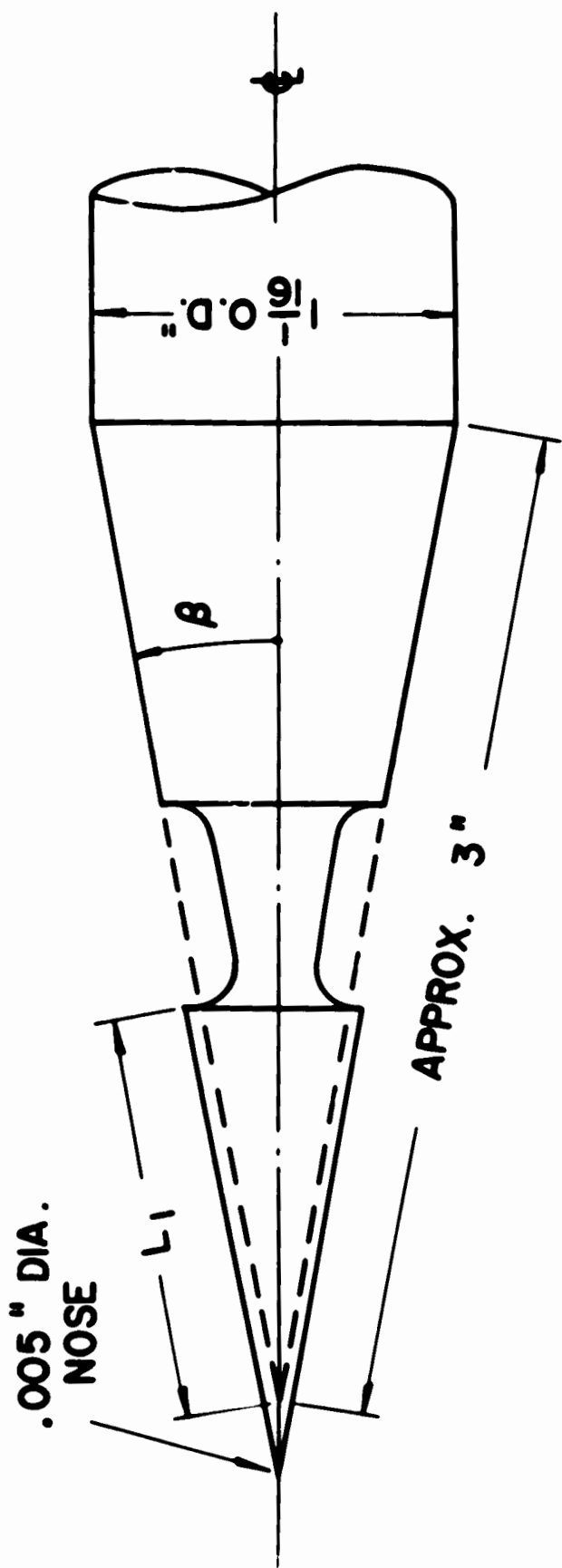
- (i) Schlieren photographs
- (ii) Hot-wire surveys
- (iii) Total-head surveys
- (iv) Applicability of a laminar similarity law  
to the measured pressure distribution
- (v) Measurements of the plenum chamber temperature  
near the end of a wind-tunnel run for small values of  $m_1$
- (vi) Measurements of the heat transfer rate some distance  
downstream of the reattachment shoulder.

No single piece of evidence was regarded as conclusive. However, on the basis of all the information taken together, it was concluded that mass injection does not have a drastic effect on the transition Reynolds number in these cavity flows. At the highest mass injection rate (regarded as unrealistically high for the present configuration), the transition Reynolds number certainly appeared to have been reduced, but this reduction was by less than a factor of two. No order of magnitude reductions were observed.

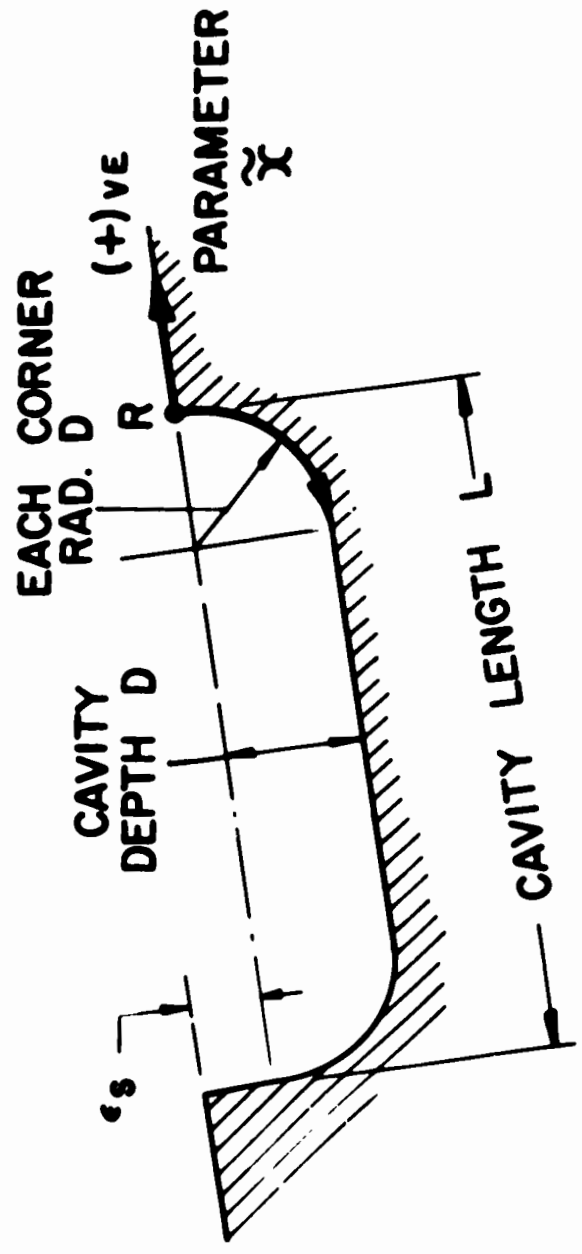
The present experimental investigation lay, for the most part, well outside the region studied by Chapman in Reference 1. The primary interest of the present work was in regions specifically excluded by Chapman in his theoretical analysis. However, the main point of the theory with regard to mass injection -- that mass injection has a pronounced effect in reducing cavity wall heat transfer rates -- agrees with the conclusions of the present report. In addition, the required amounts of mass injection given by Chapman's theory were of the correct order.

#### REFERENCES

1. Chapman, D. R.: A Theoretical Analysis of Heat Transfer in Regions of Separated Flow. NACA TN 3792, October 1956.
2. Nicoll, K. M.: An Experimental Investigation of Laminar Hypersonic Cavity Flows. Ph.D. Thesis, Princeton University, 1963.
3. Nicoll, K. M.: A Study of Laminar Hypersonic Cavity Flows. AIAA Journal, Vol. 2, No. 9, September 1964, pp. 1535-1541.
4. Henderson, A. and Braswell, D. O.: Charts for Conical and Two-dimensional Oblique-shock Flow Parameters in Helium at Mach Numbers from About 1 to 100. NASA TN D-819, June 1961.
5. Nicoll, K. M.: Investigation of the Laminar Boundary Layer on a Flat Plate in Helium Using the Crocco Method. PUAED Report 590, December 1961. Also published as ARL 62-345, May 1962.
6. Nicoll, K. M.: Design Criteria and Experimental Technique for a Study of a Hypersonic Cavity Flow with Mass Injection. Princeton University, Dept. of Aerospace & Mech. Sciences, Gas Dynamics Laboratory Internal Memorandum 6, December 1964.
7. Bogdonoff, S. M. and Hammitt, A. G.: The Princeton Helium Hypersonic Tunnel and Preliminary Results above  $M = 11$ . PUAED Report 260, June 1954. Also published as WADC TN 54-124.



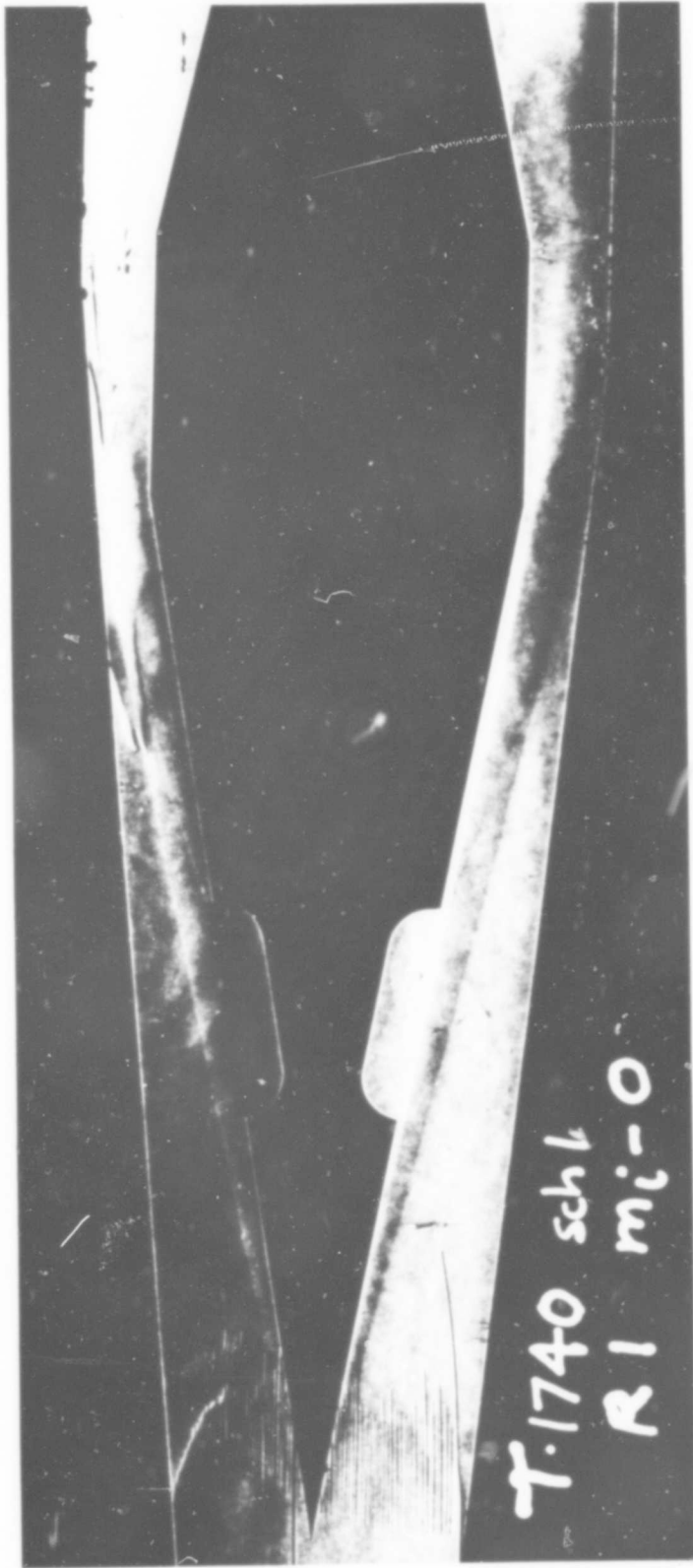
ALL MODELS AXISYMMETRIC



- $L_1 = 1\frac{1}{4}$ "
- $L = 5/8$ "
- $D = 1/8$ "
- $\beta = 10^\circ$
- $\beta_s = 0, .01$   
.02 AND  
.03 INCHES

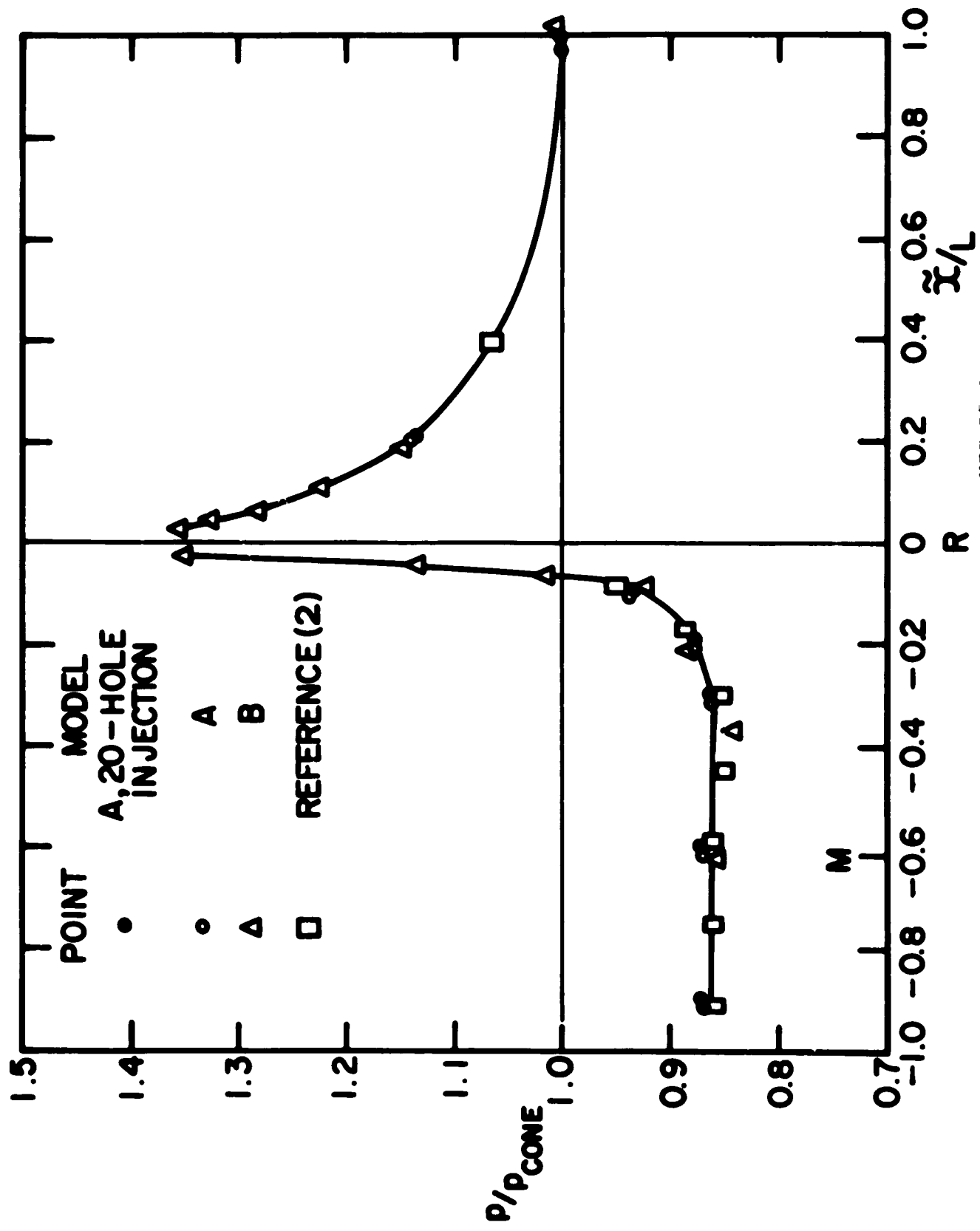
XII B5-1

Figure 1. Wind-tunnel model geometry.



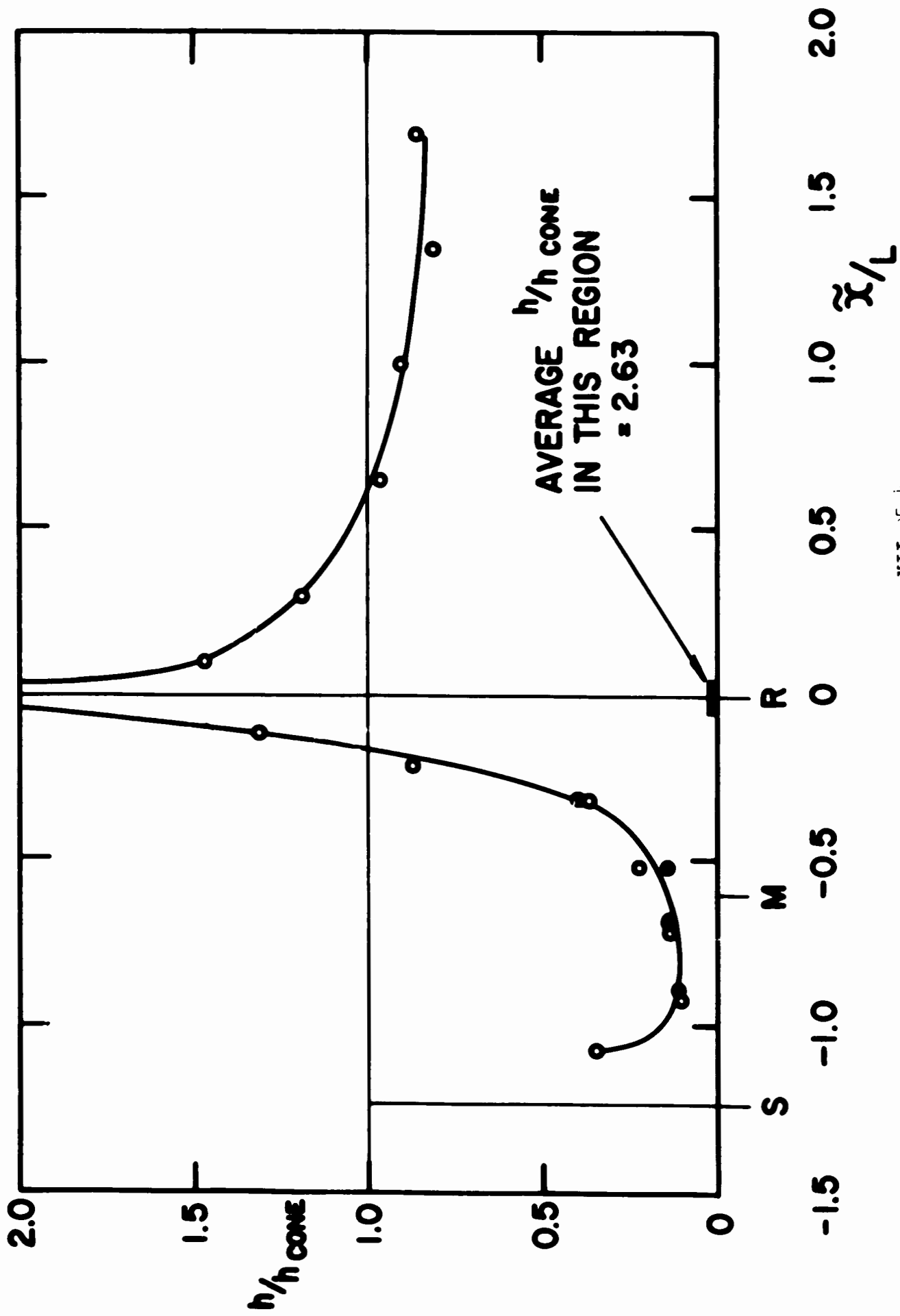
XII B5-2

Figure 2. Schlieren photograph of flow over basic cavity model at  $P_0 = 400$  psia., with  $m_1 = \epsilon_s/L = 0$ .



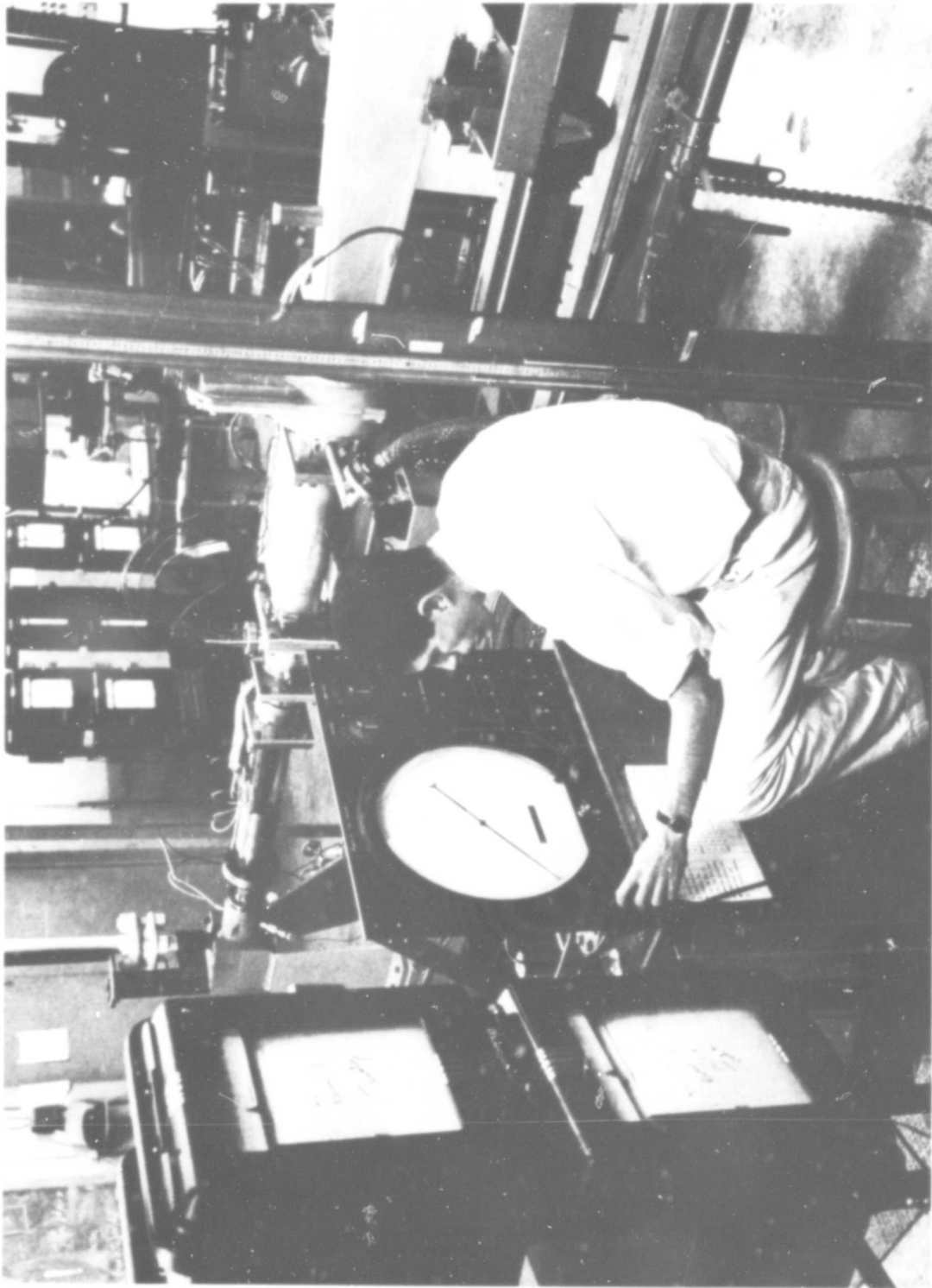
XII B5-3

Figure 3. Pressure distribution for  $m_1 = \epsilon_s/L = 0$ .



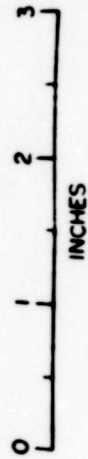
XII B5-4

Figure 4. Distribution of heat transfer coefficient for  $\pi_1 = \epsilon_3/L = 0$ .



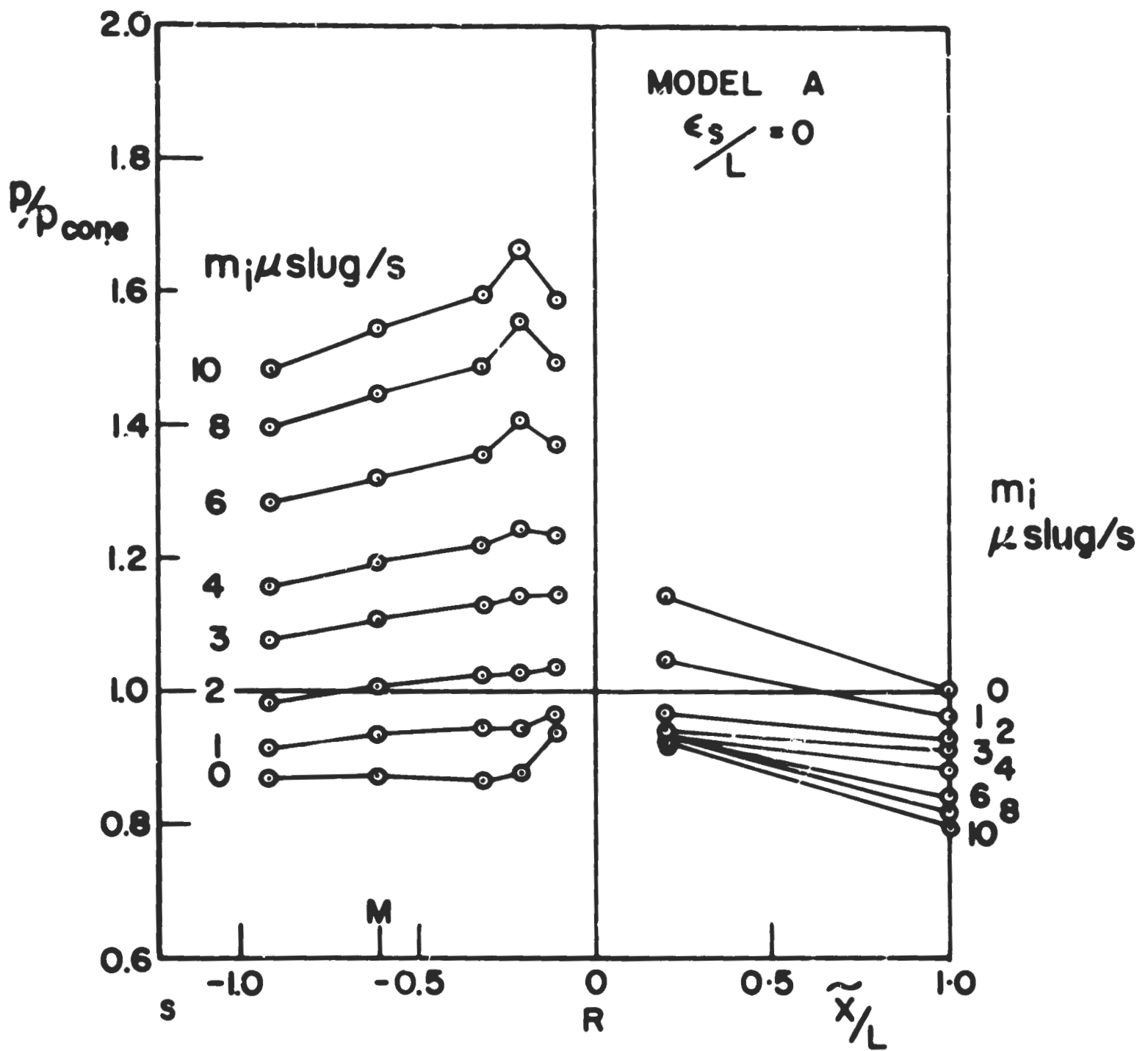
XII B5-5

Figure 5. Photograph of mass-flow measurement plant from the front, with 3-inch helium hypersonic wind-tunnel in the background.



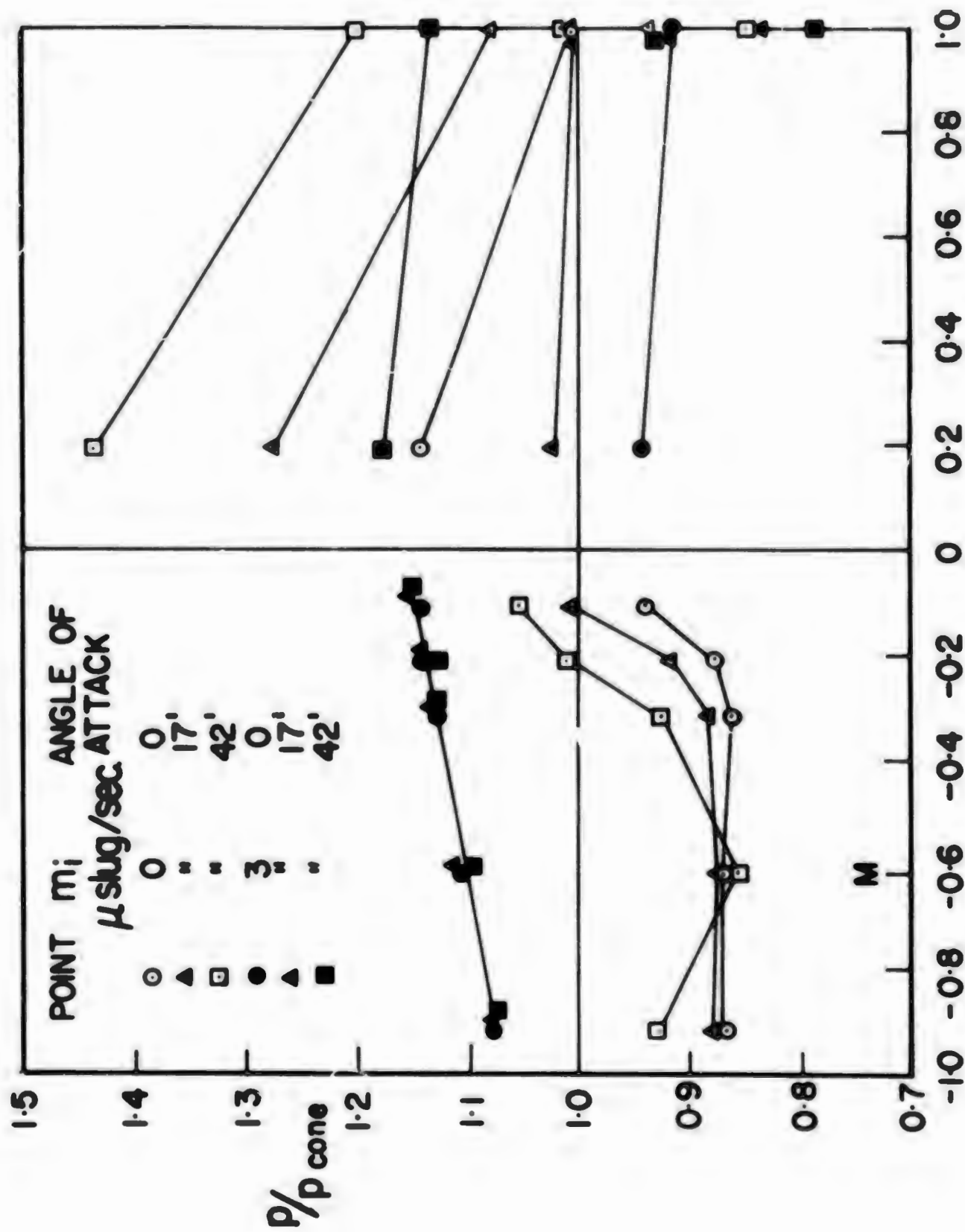
XII B5-6

Figure 6. Wind-tunnel models. From left to right, heat transfer model, pressure model B and pressure model A.



XII B'

Figure 7. Pressure distribution on model A, with  $\epsilon_s/L = 0$ .



R X = B5-8  $\bar{x}/L$   
 Figure 8. Effects of angle of attack on windward-side pressure distribution; model A with  $\epsilon_g/L = 0$ .

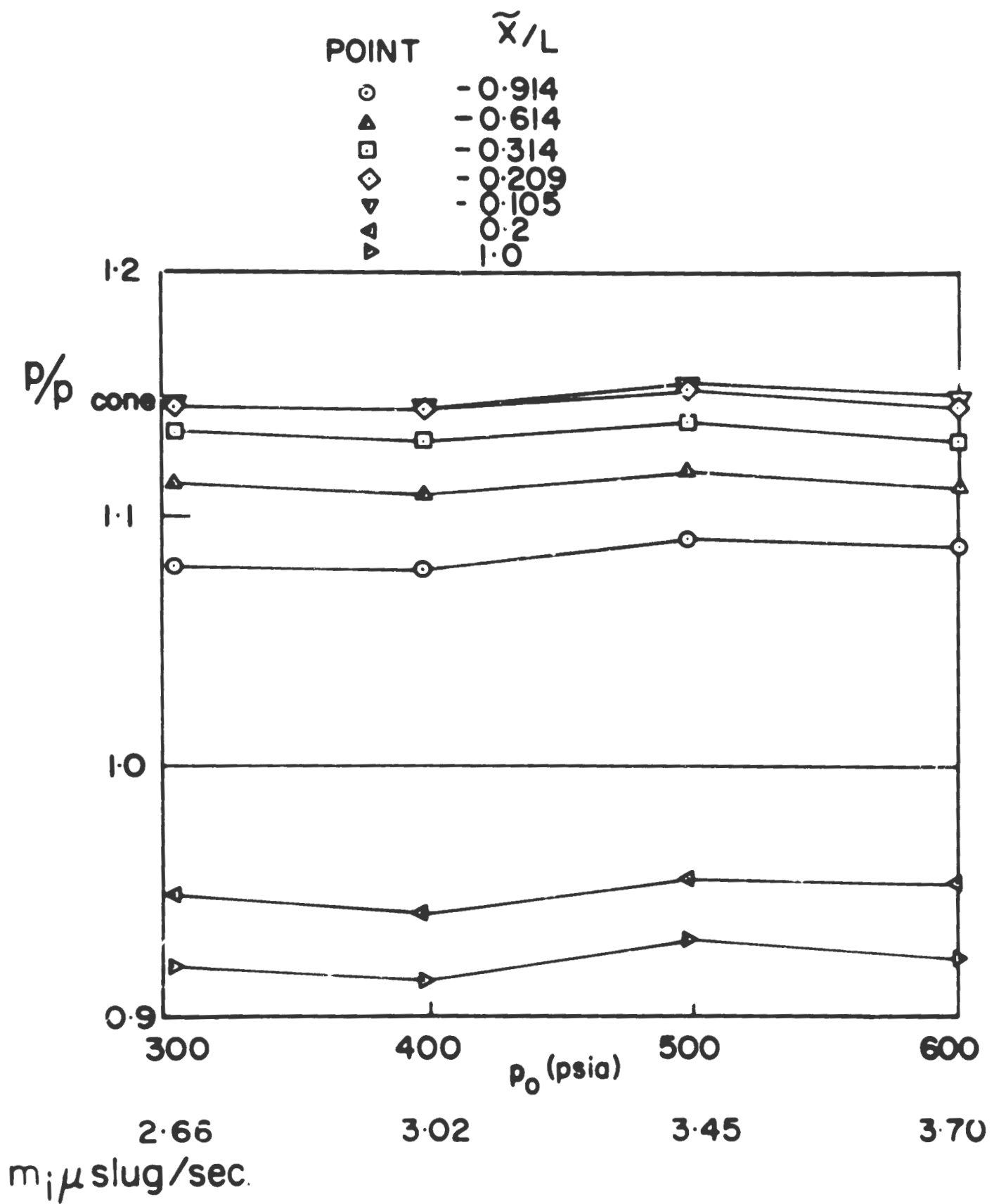


Figure 1. Laminar similarity check.

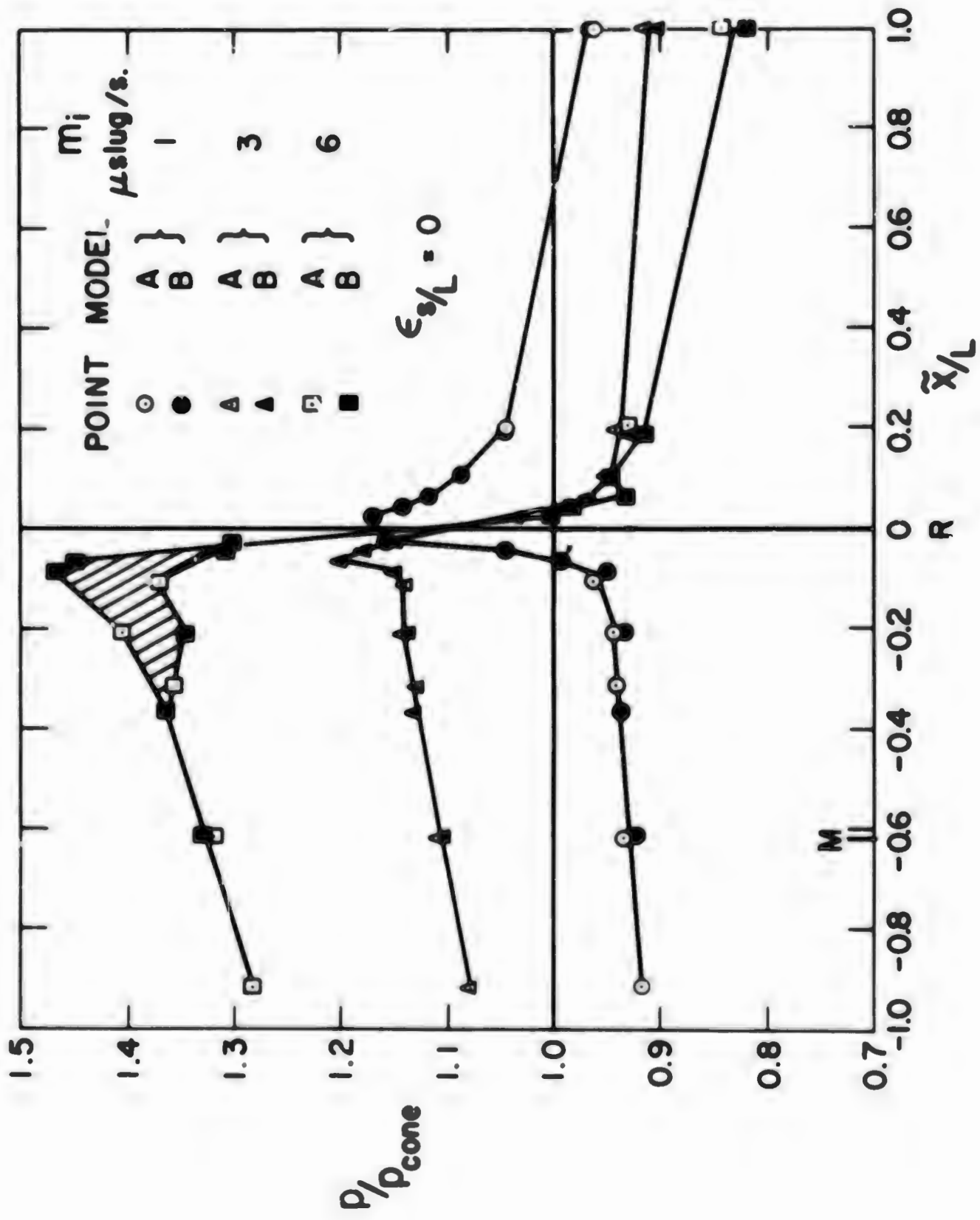
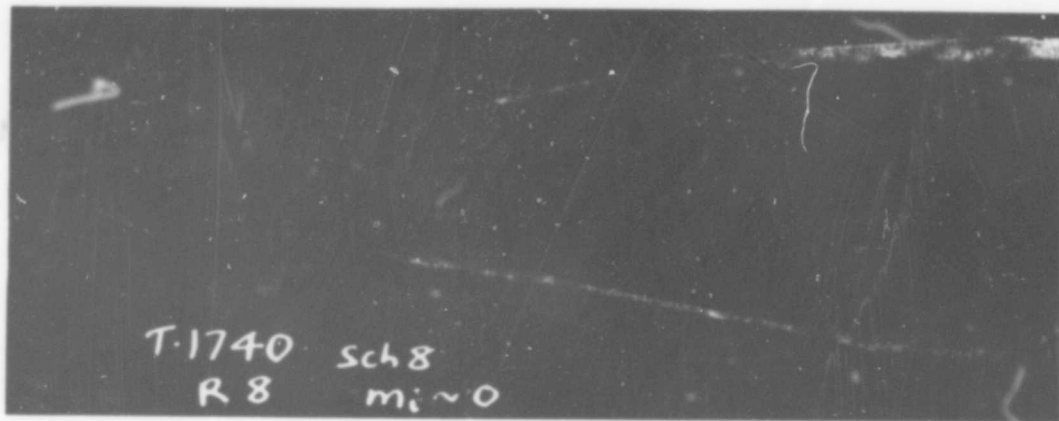
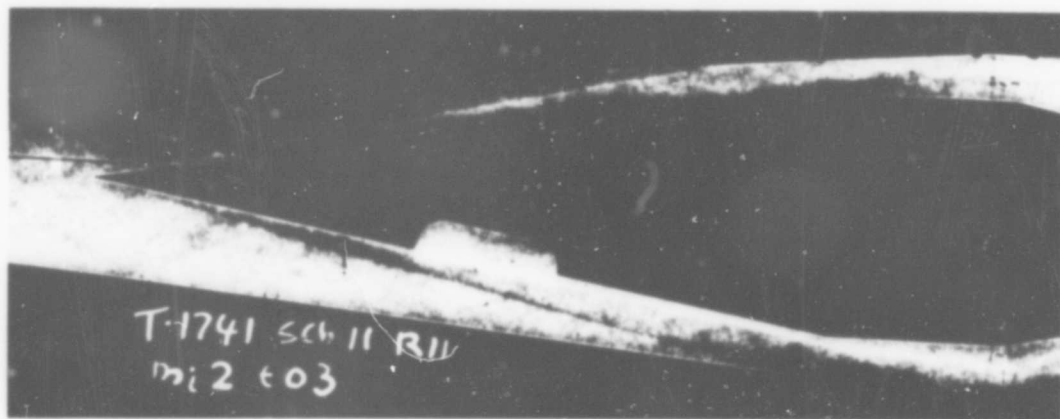


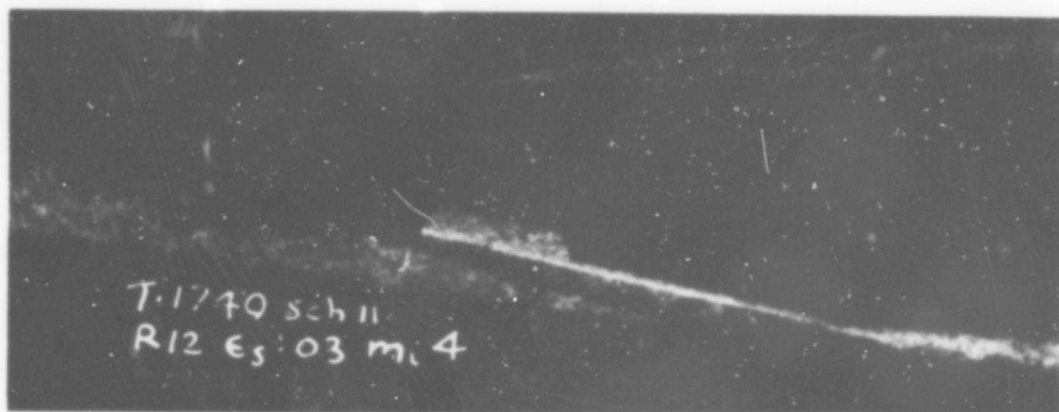
Figure 10. Comparison of pressure distributions measured by models A and B, with  $\epsilon_s/L = 0$ .



(a)  $m_1 = 0$ ,  $\epsilon_S/L = 0.048$ .



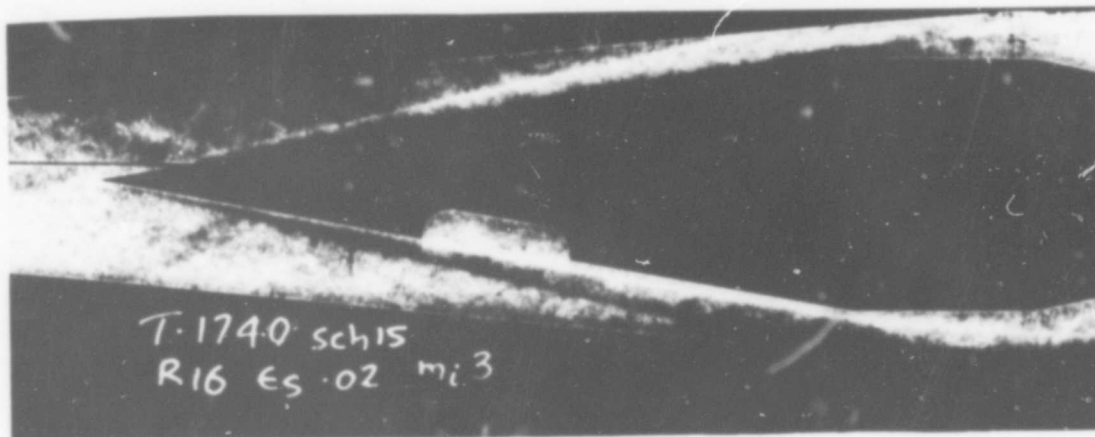
(b)  $m_1 = 2 \mu\text{slug/second}$ ,  $\epsilon_S/L = 0.048$ .



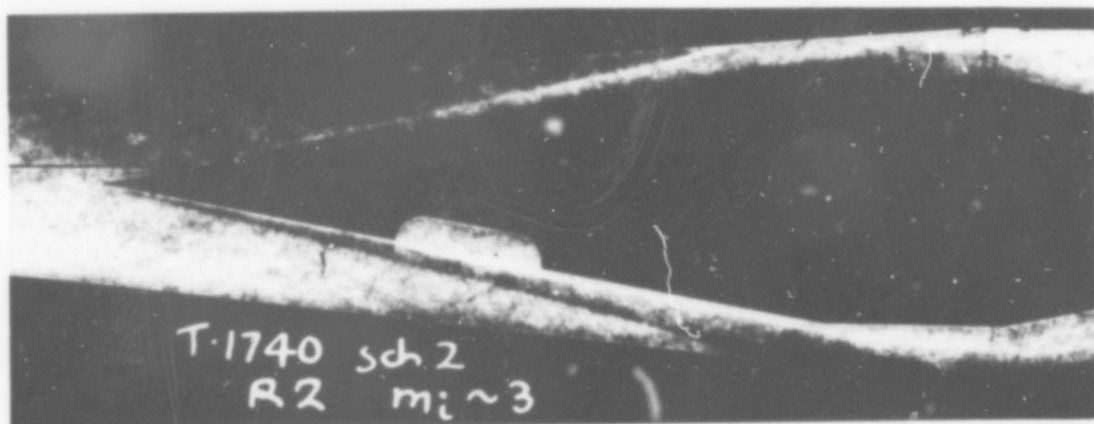
(c)  $m_1 = 4 \mu\text{slug/second}$ ,  $\epsilon_S/L = 0.048$ .

XII B5-11

Figure 11. Typical schlieren photographs of flow over model B with various values of  $m_1$  and  $\epsilon_S/L$ .



(d)  $m_1 = 3 \mu\text{slug/second}$ ,  $\epsilon_s/L = 0.032$ .



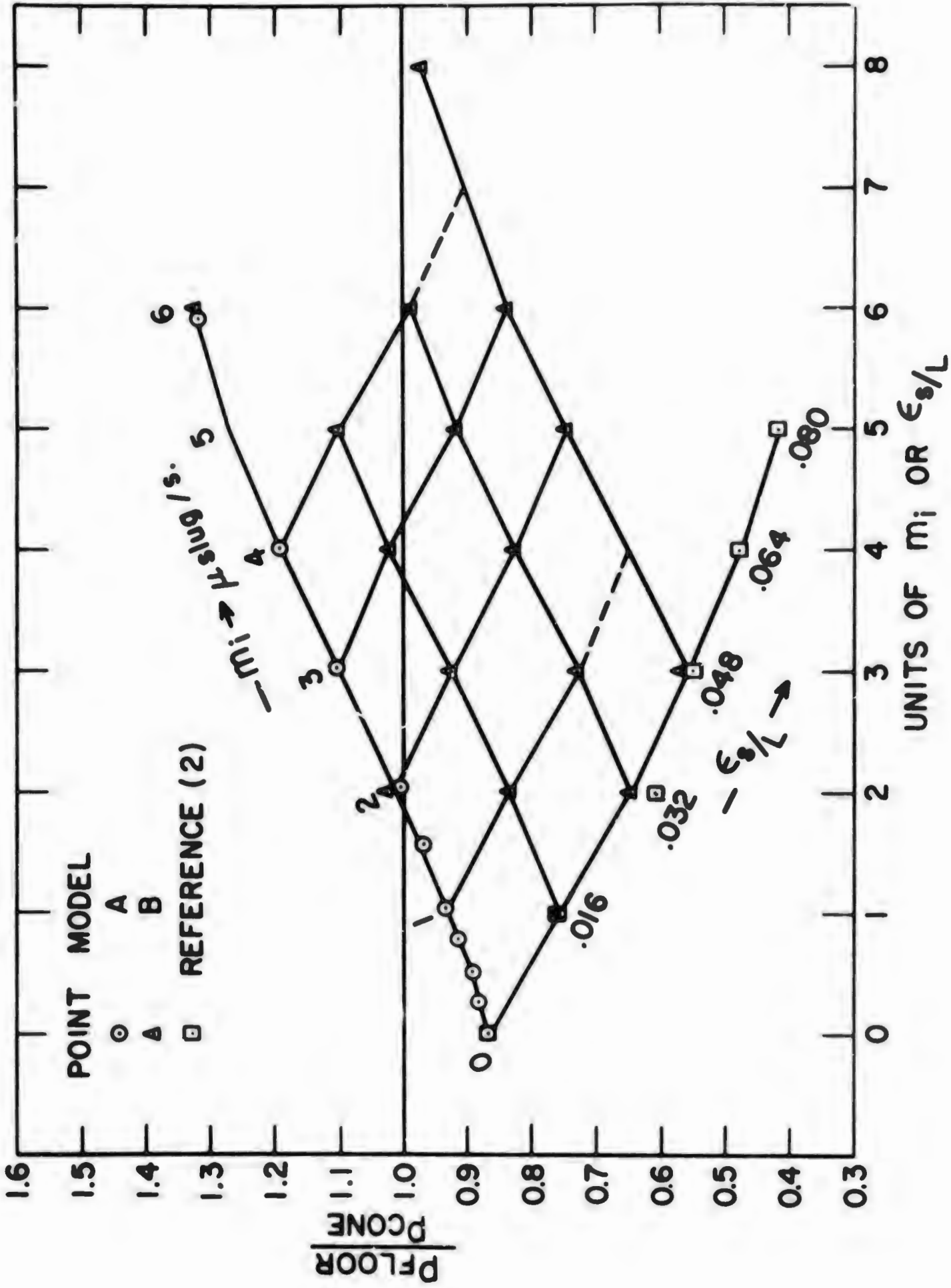
(e)  $m_1 = 3 \mu\text{slug/second}$ ,  $\epsilon_s/L = 0$ .



(f)  $m_1 = 10 \mu\text{slug/second}$ ,  $\epsilon_s/L = 0$ .

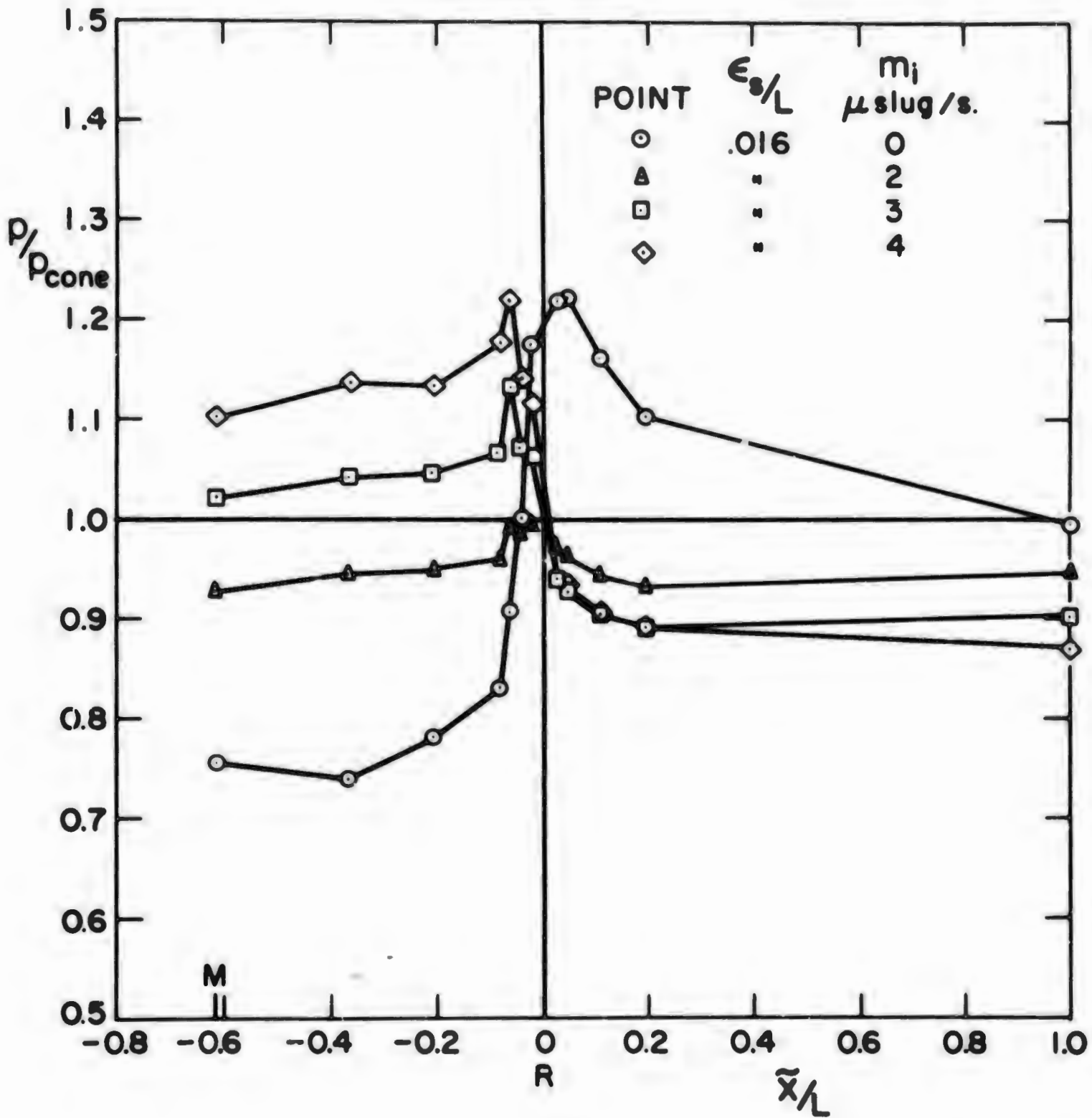
XII B5-12

Figure 11. (continued).



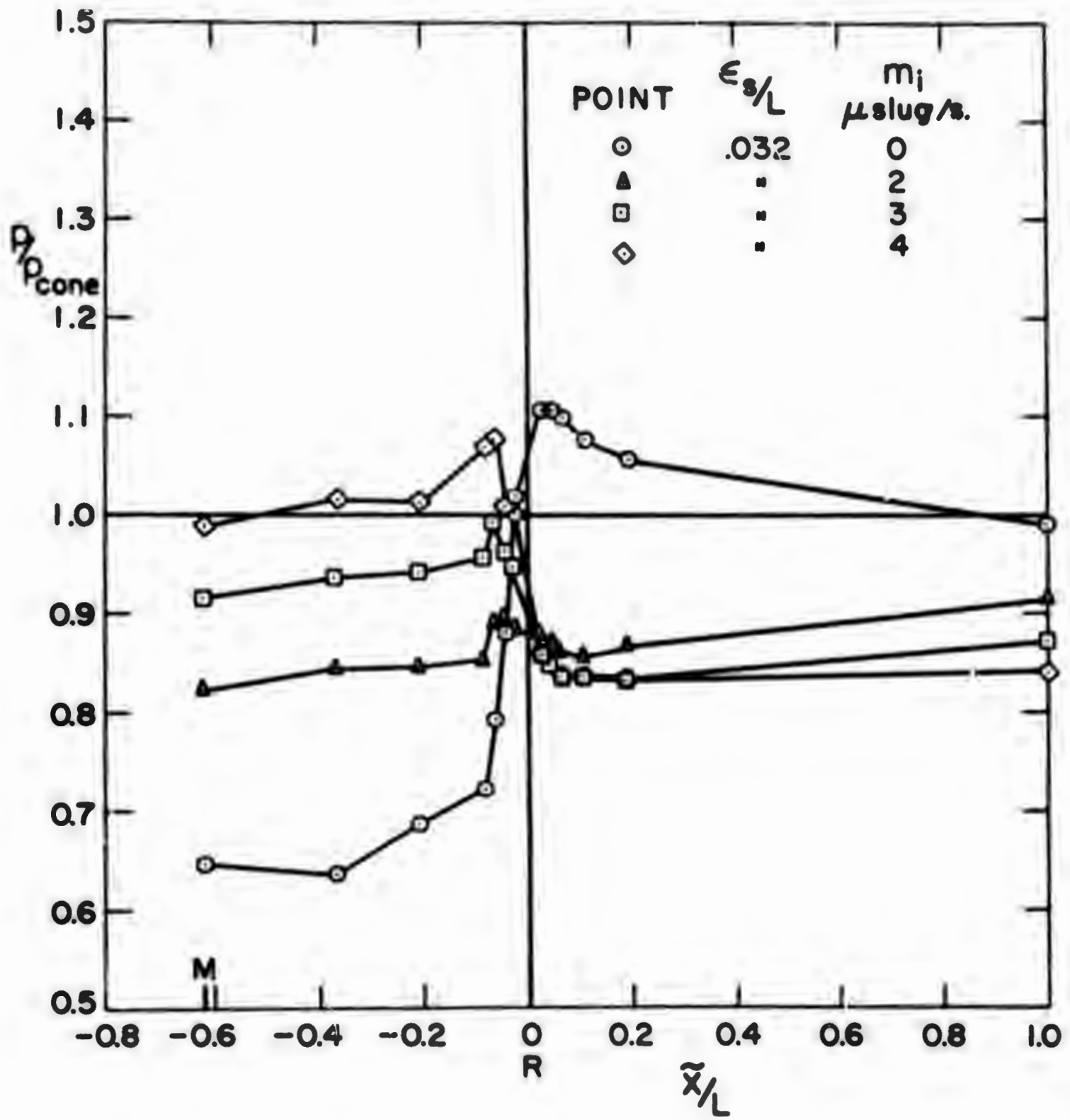
XII B-1J

Figure 12. Measured pressure at mid-point of cavity floor, against  $m_i$  and  $\epsilon_s/L$ .



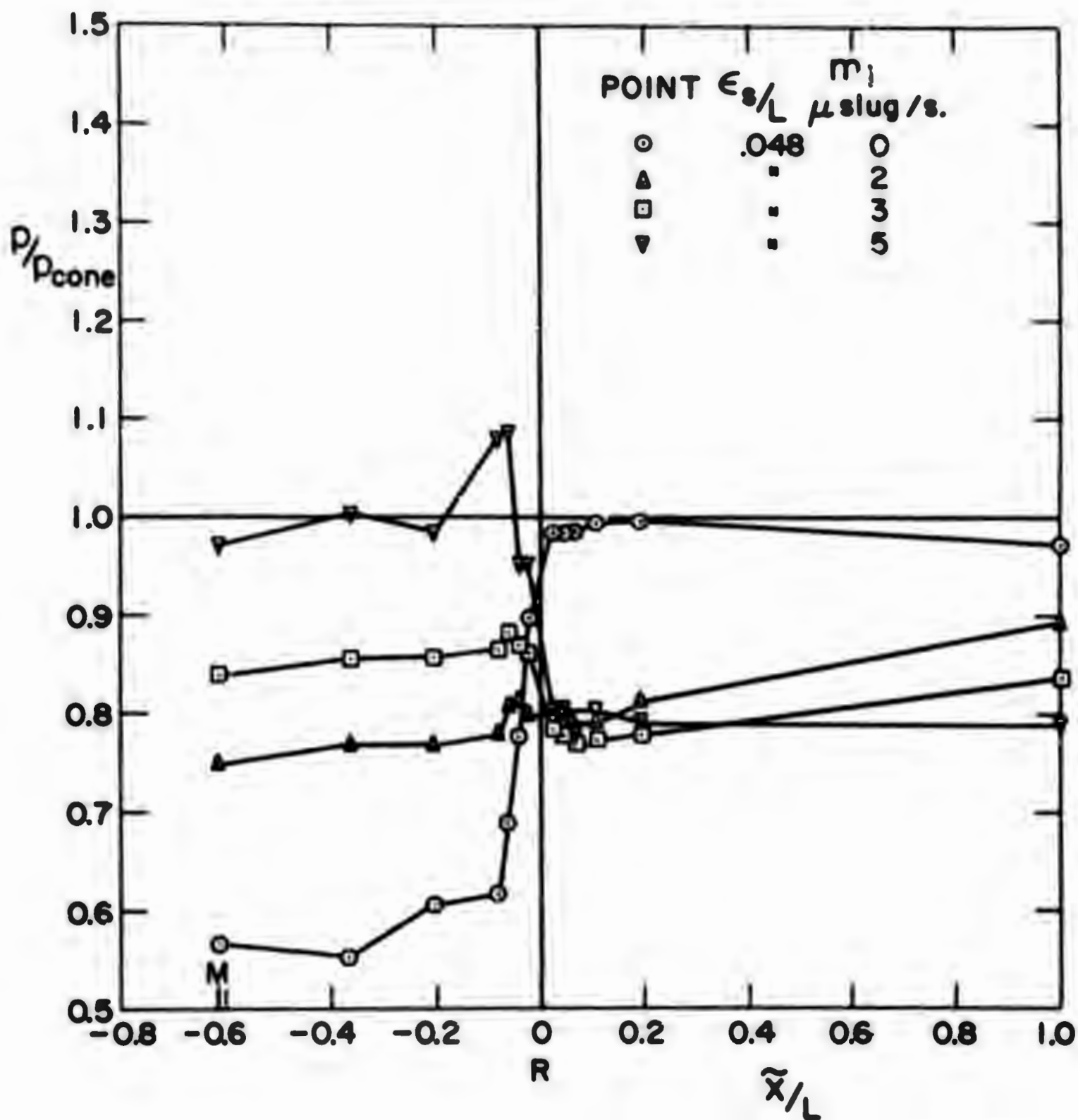
XII B' -14

Figure 13. Pressure distribution on model B,  
 $\epsilon_s/L = 0.016$ .



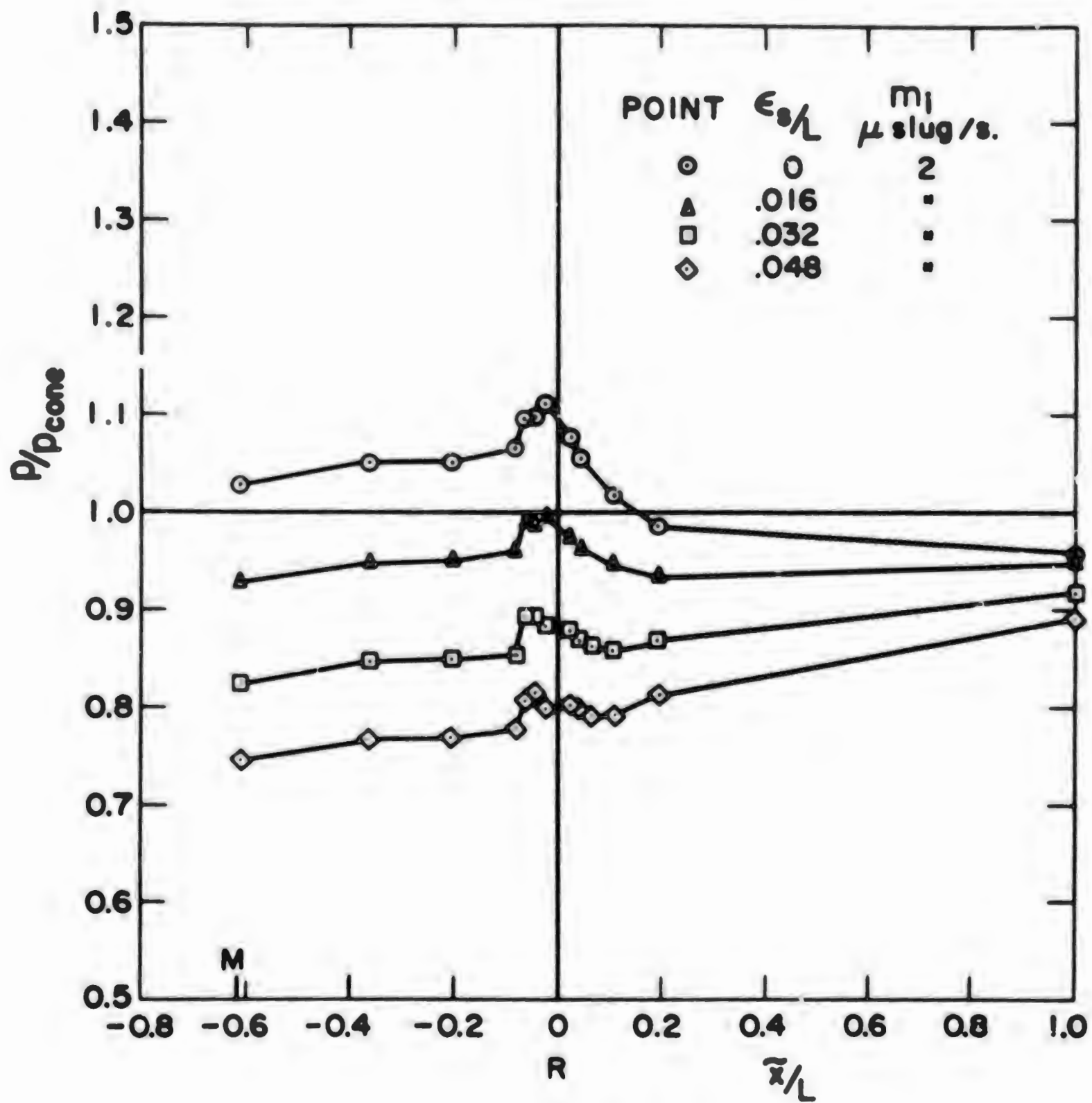
XII B5-15

Figure 14. Pressure distribution on model B,  
 $\epsilon_s/L = 0.032$ .



XII B5-16

Figure 15. Pressure distribution on model B,  
 $\epsilon_s/L = 0.048$ .



X 11 - 11

Figure 16. Pressure distribution on model B,  
 $m_1 = 2$  microslugs/second.

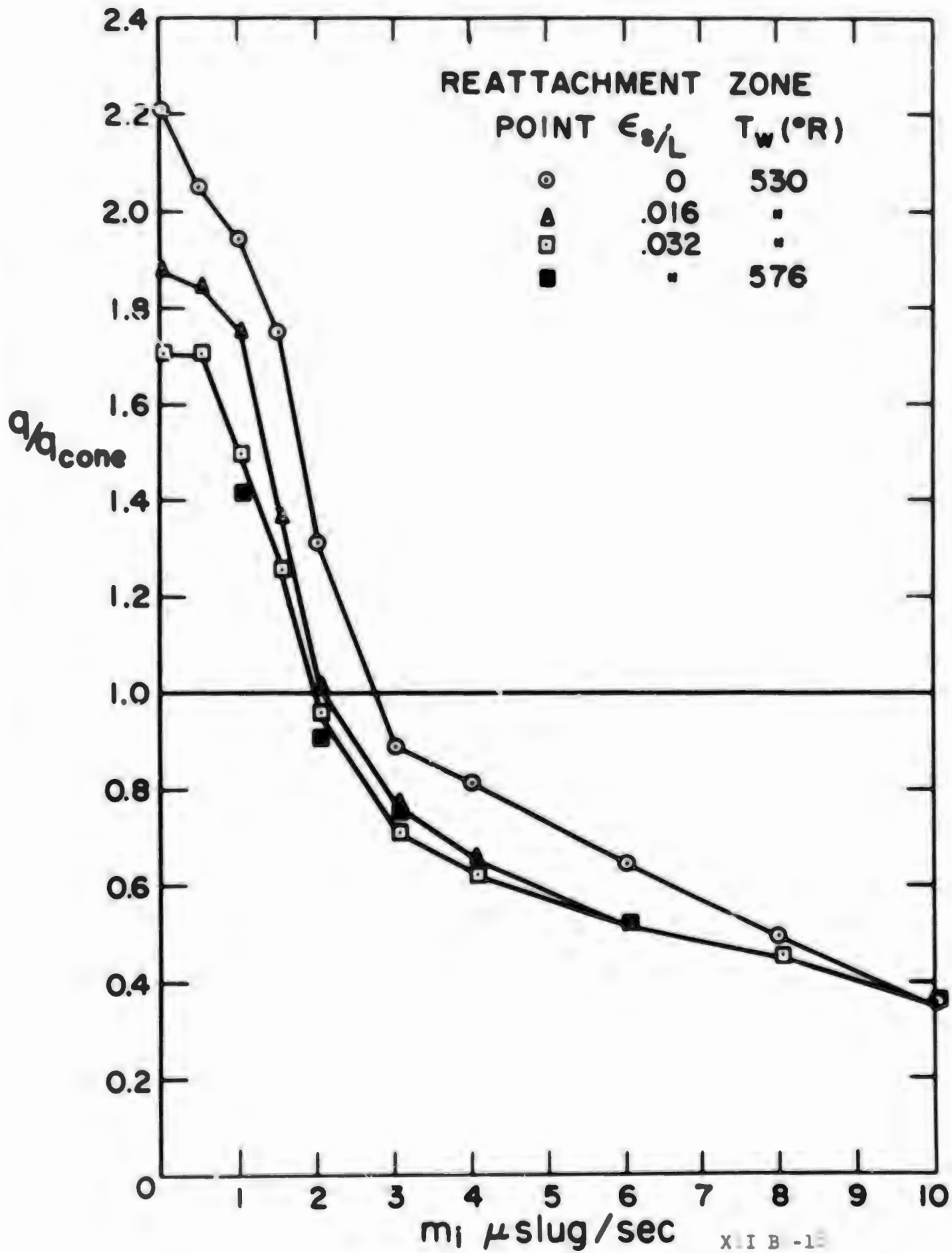
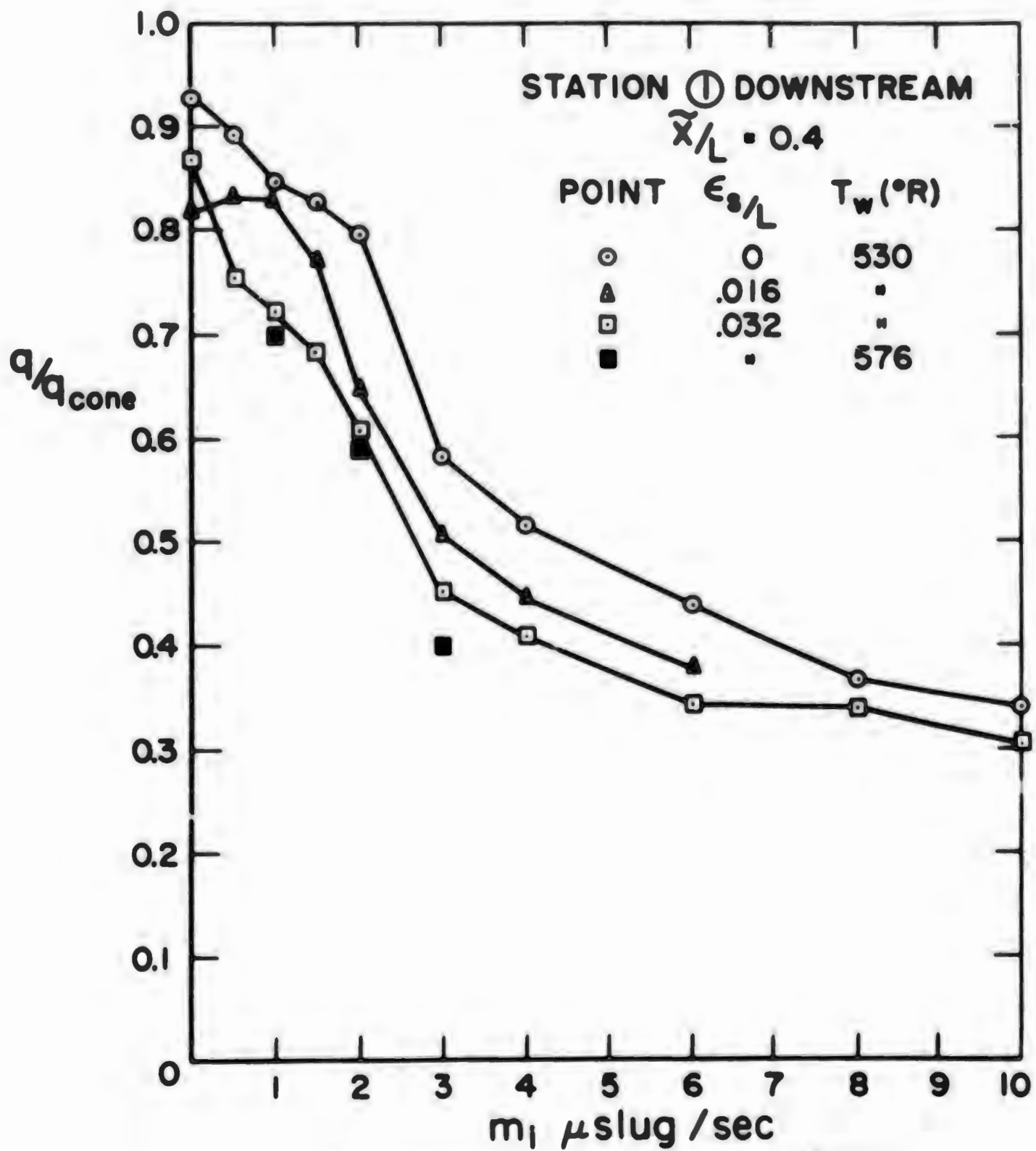


Figure 17. Effect of mass injection on average heat transfer rate at cavity reattachment shoulder.



X I B5-19

Figure 18. Effect of mass injection on heat transfer rate at downstream station (1).

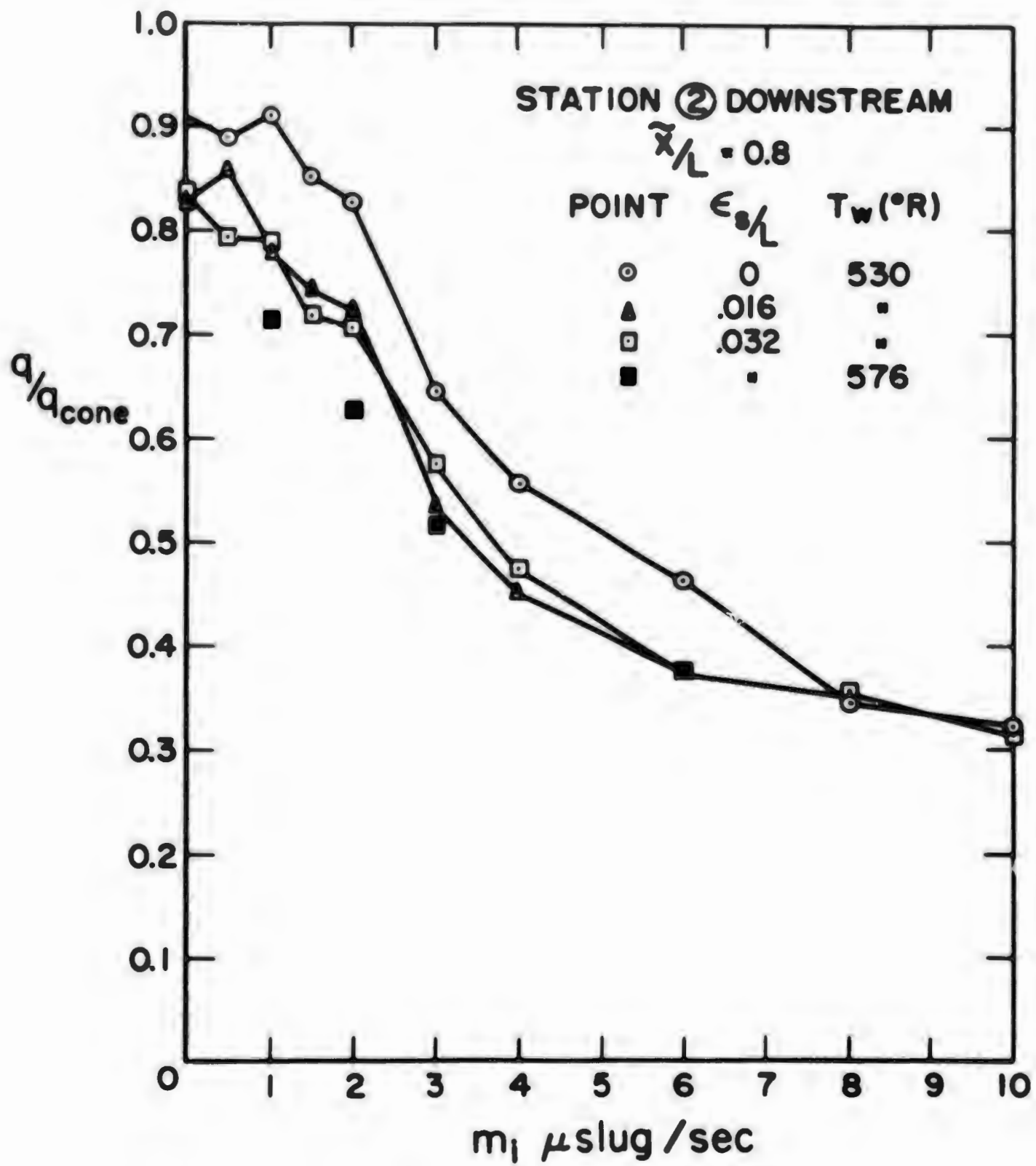


Figure 19. Effect of mass injection on heat transfer rate at downstream station (2).

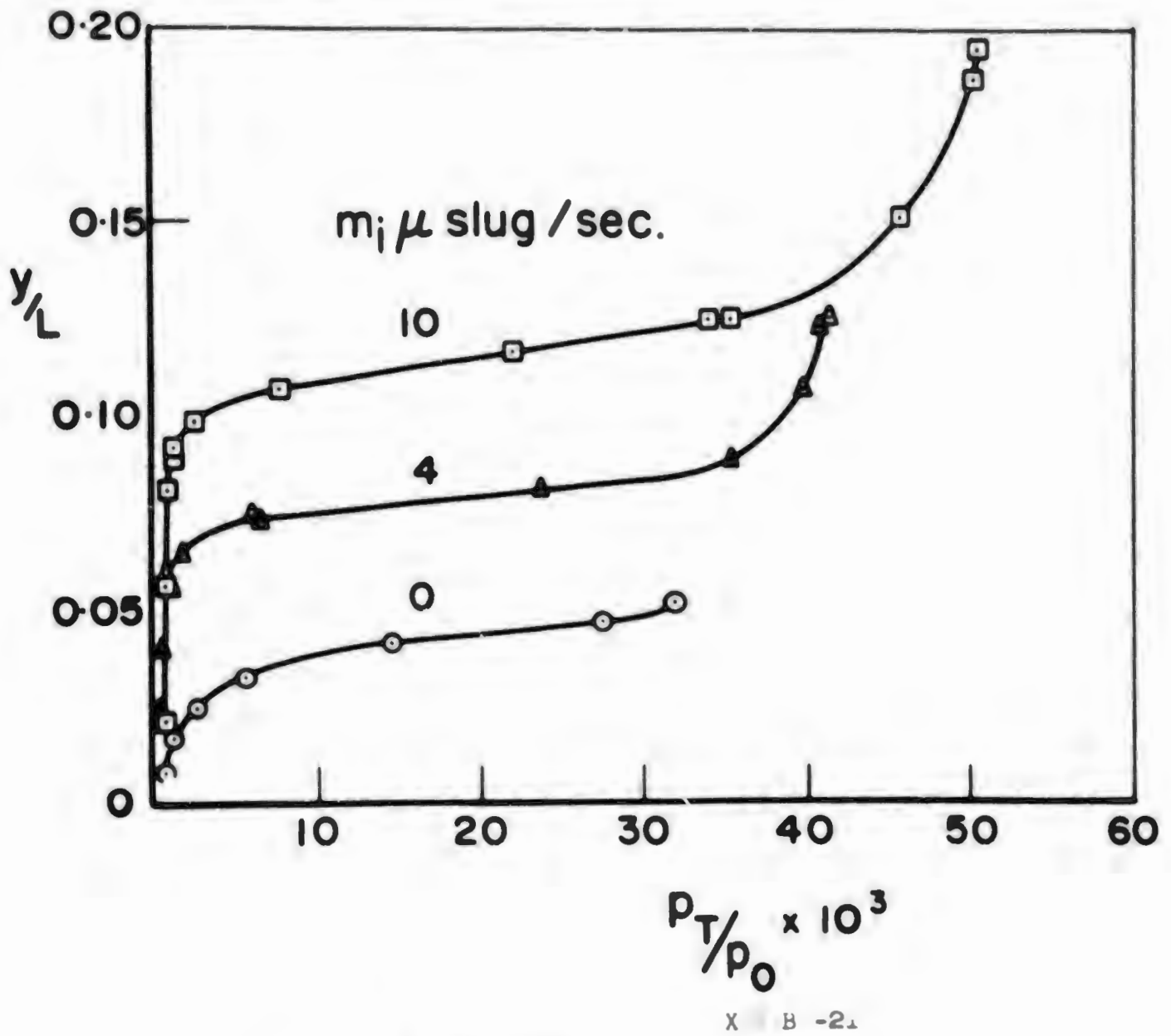
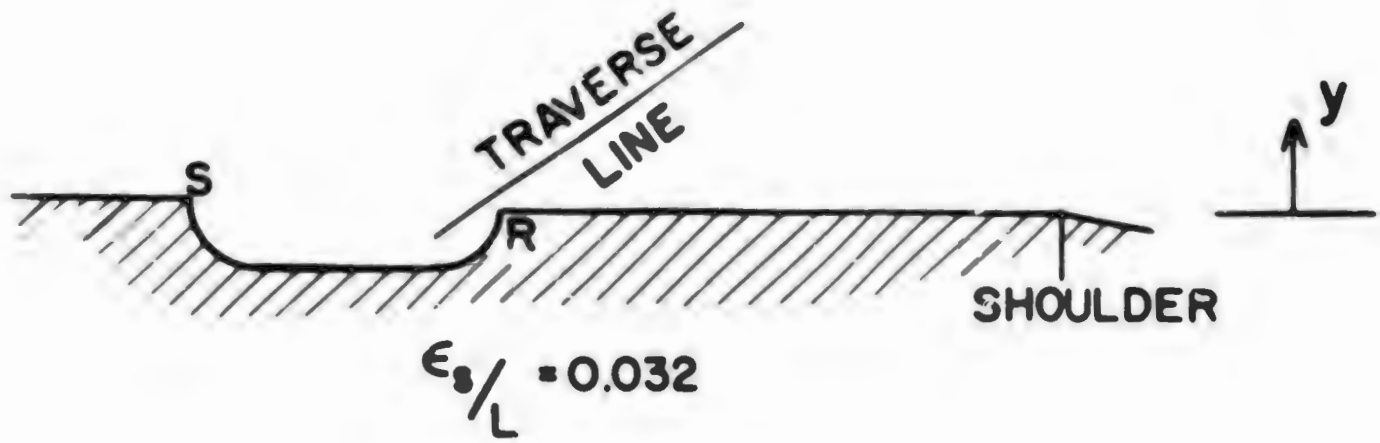
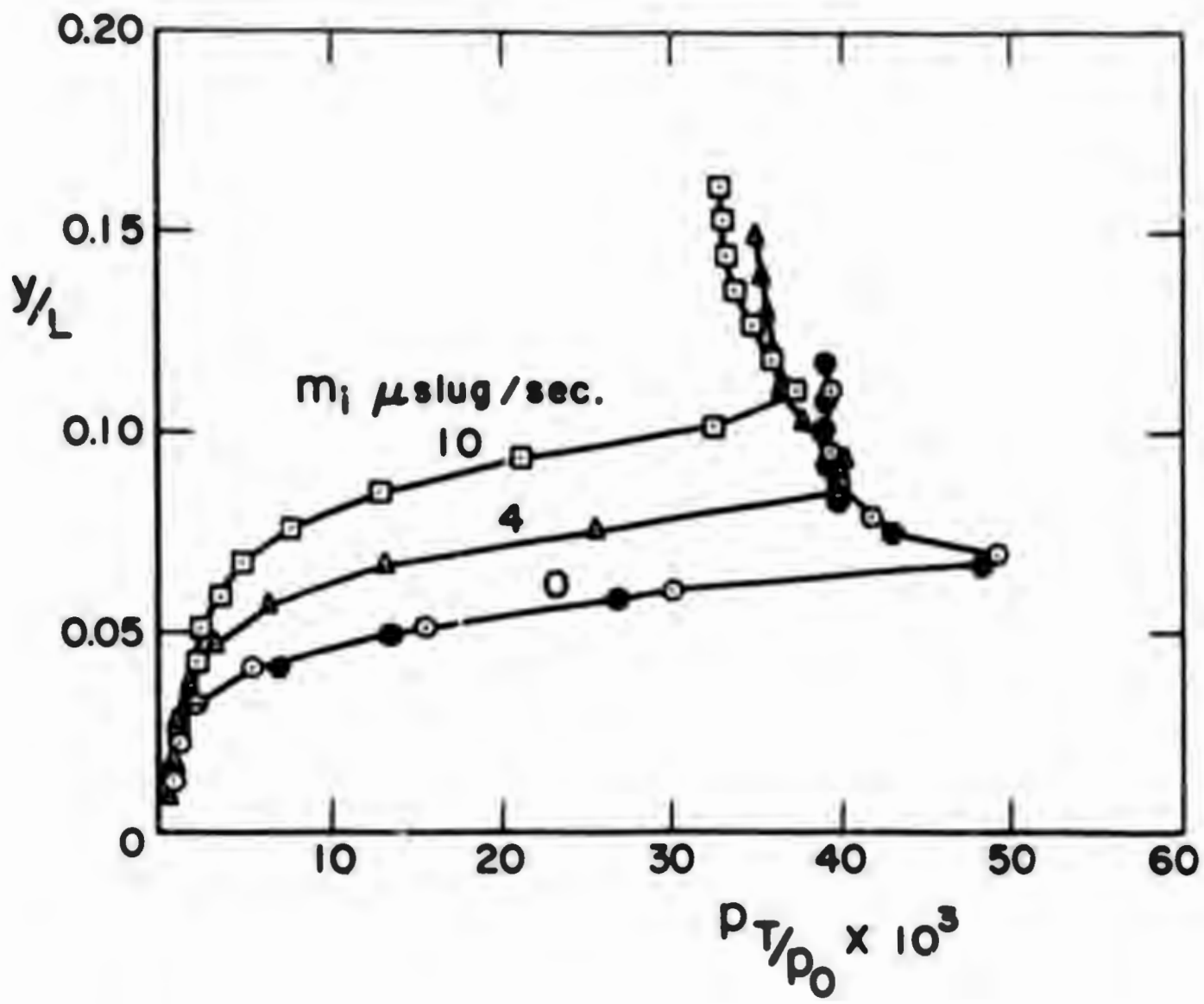
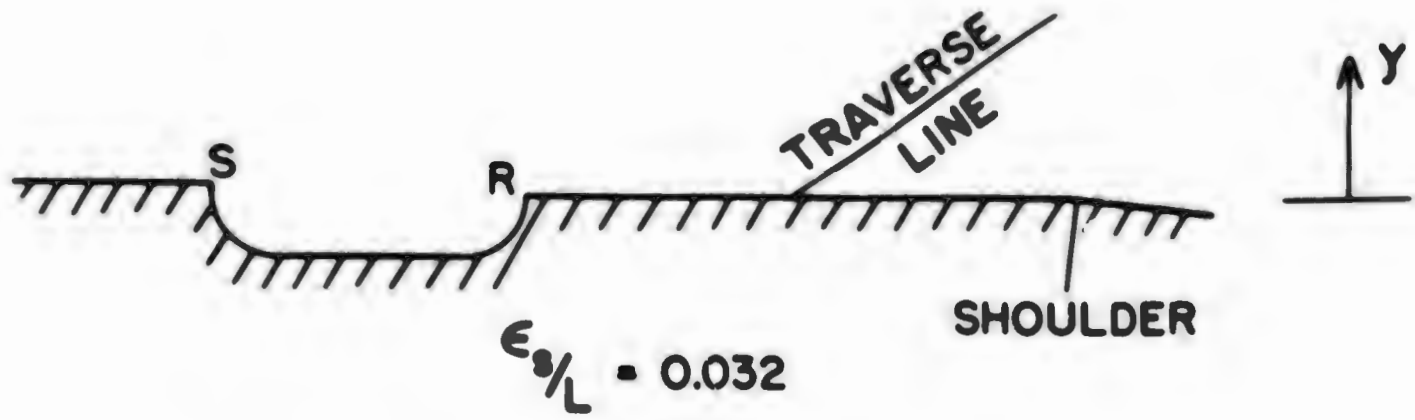
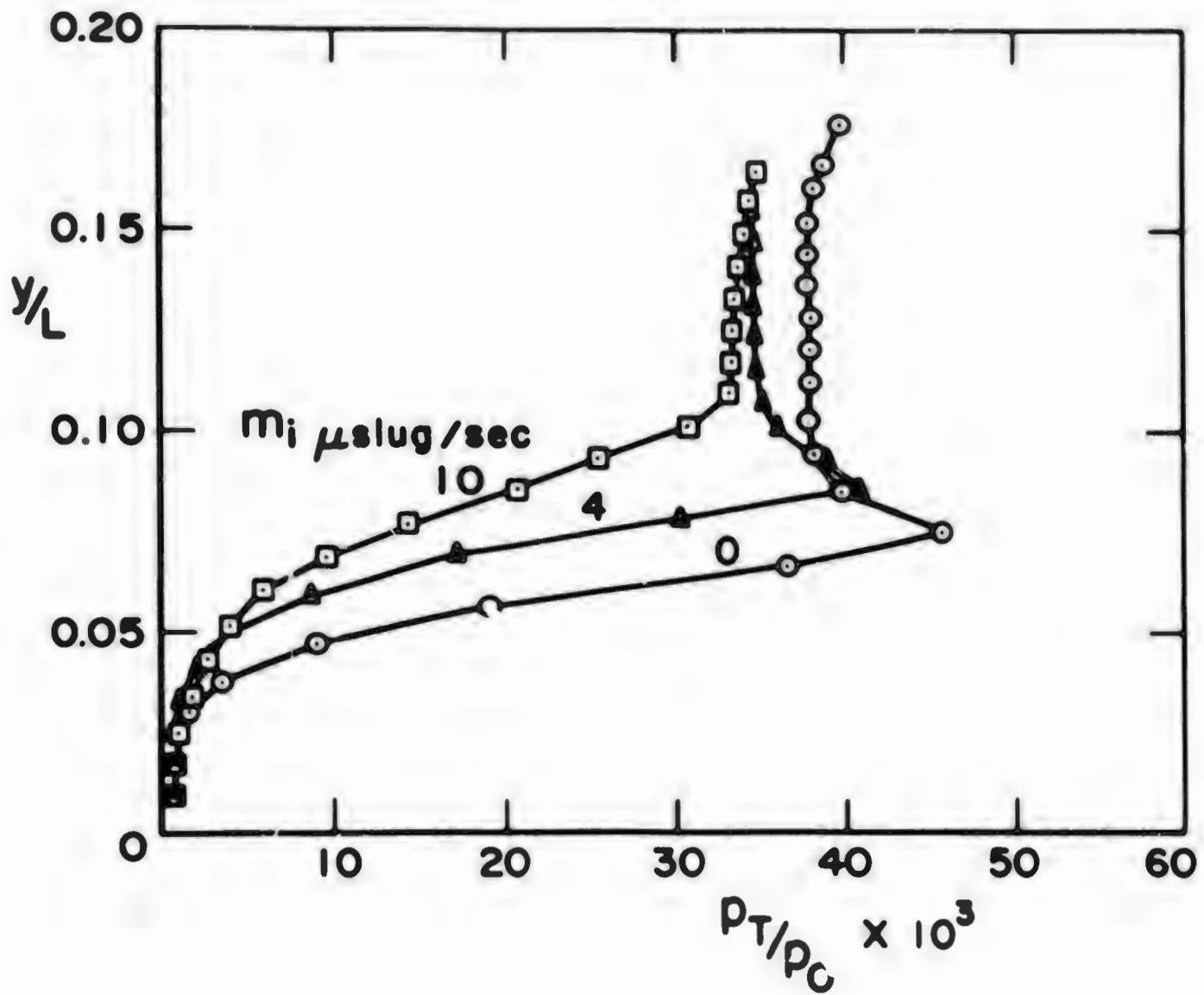
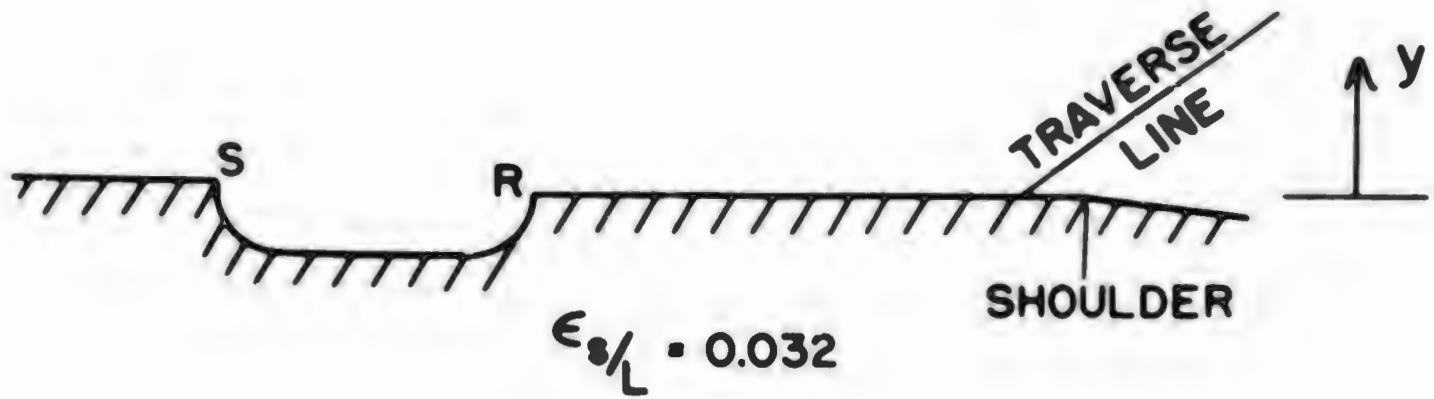


Figure 20. Total-head surveys at station near reattachment shoulder,  $\epsilon_s/L = 0.032$ .



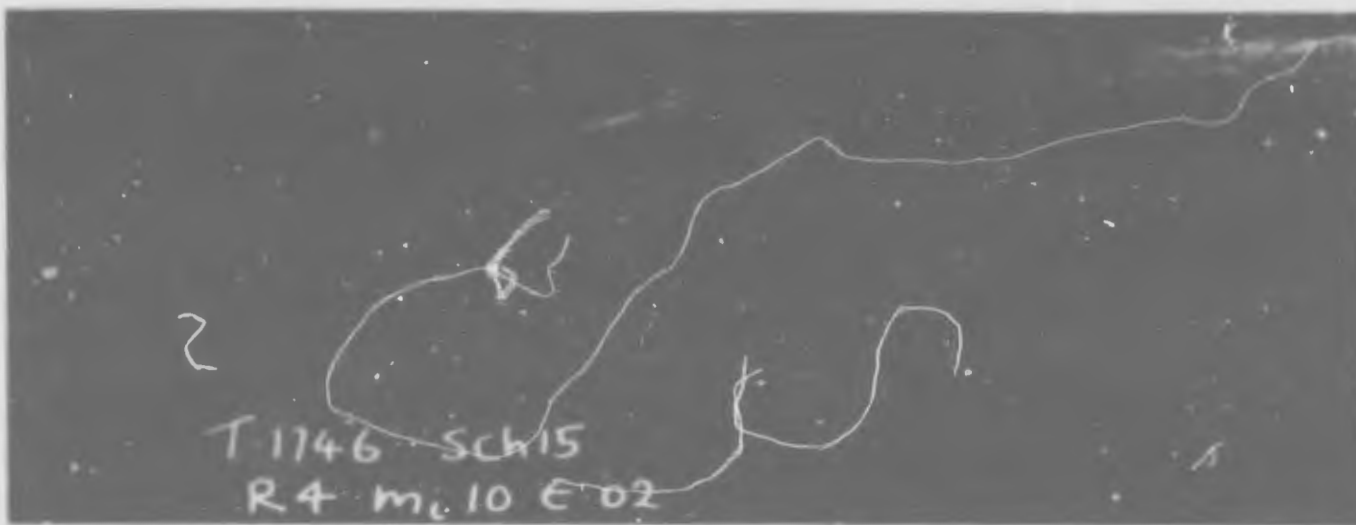
XII B5 -22

Figure 21. Total-head surveys, downstream station,  $\epsilon_s/L = 0.032$ .



XII B5-23

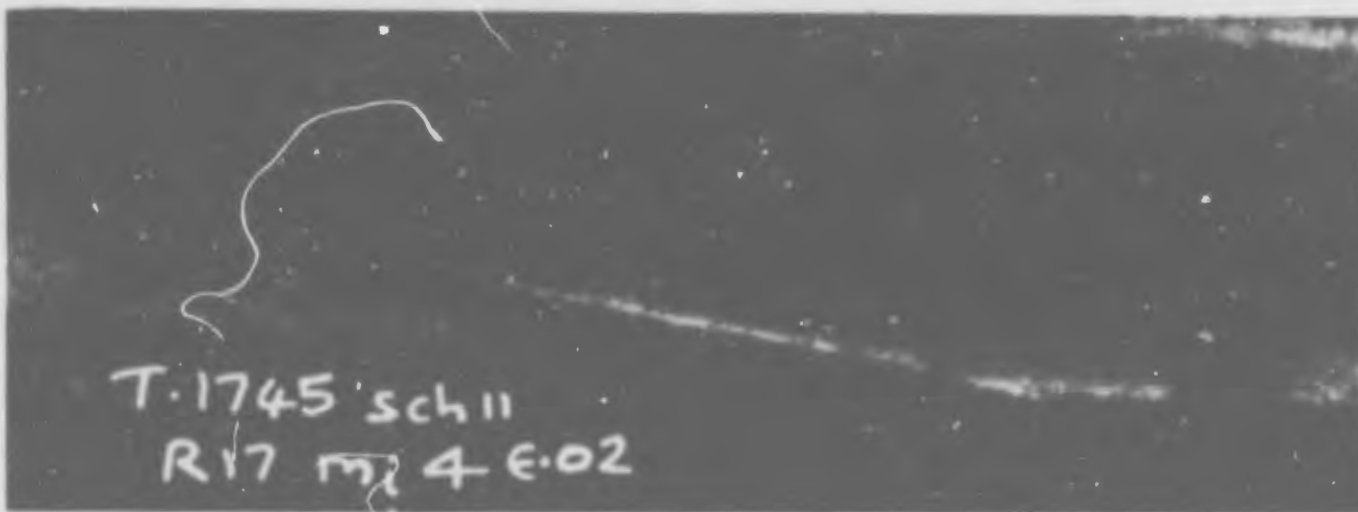
Figure 22. Total-head surveys, far downstream station,  $\epsilon_s/L = 0.032$ .



(a)  $m_1 = 10 \mu\text{slug/second}$ ,  $\epsilon_S/L = 0.032$ , middle traverse station.



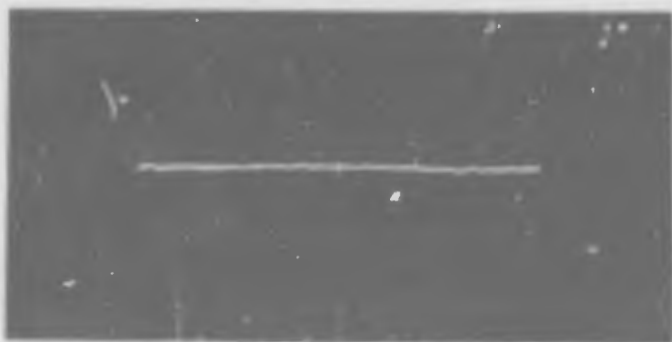
(b)  $m_1 = 10 \mu\text{slug/second}$ ,  $\epsilon_S/L = 0.032$ , rear traverse station.



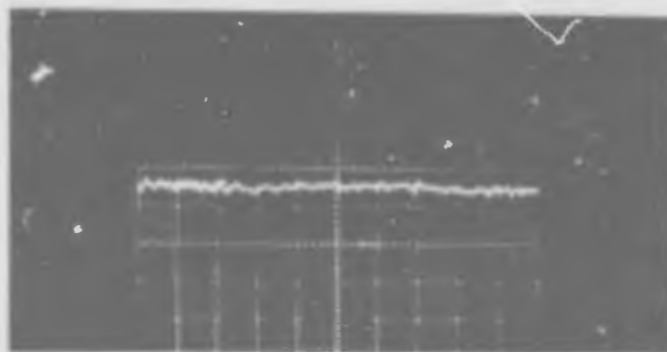
(c)  $m_1 = 4 \mu\text{slug/second}$ ,  $\epsilon_S/L = 0.032$ , downstream interference.

XII B5-24

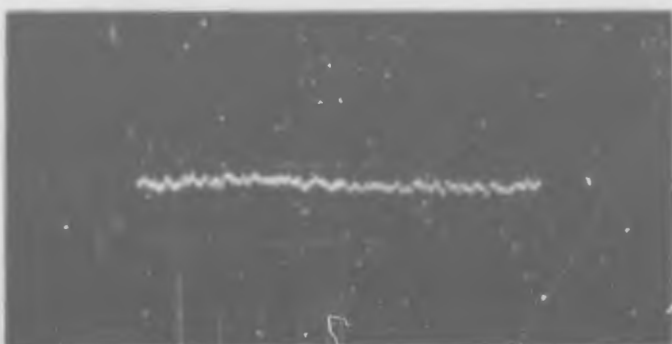
Figure 23. Schlieren photographs of total-head probe traverses and interference studies.



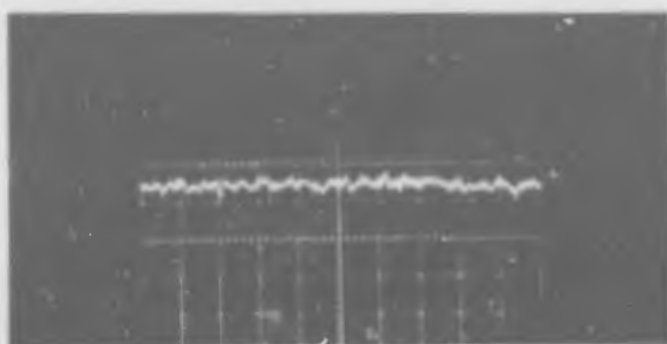
(a) Upstream traverse station.  
Just outside boundary layer.



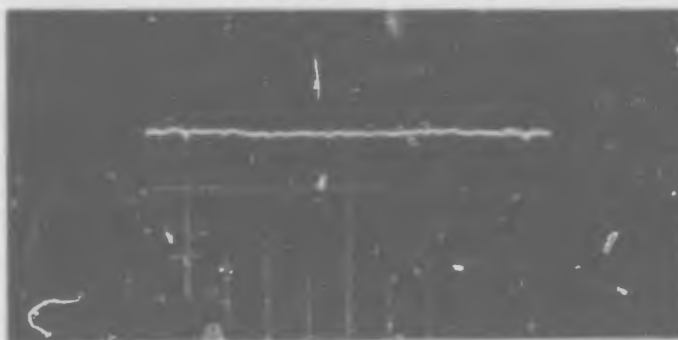
(d) Rear traverse station.  
Outside boundary layer.



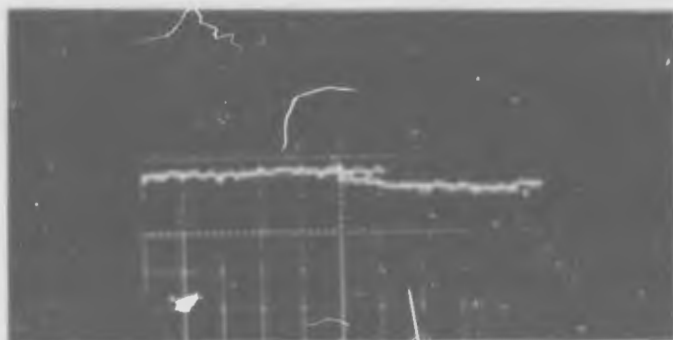
(b) Upstream traverse station.  
Maximum shear zone.



(e) Rear traverse station.  
Maximum shear zone.



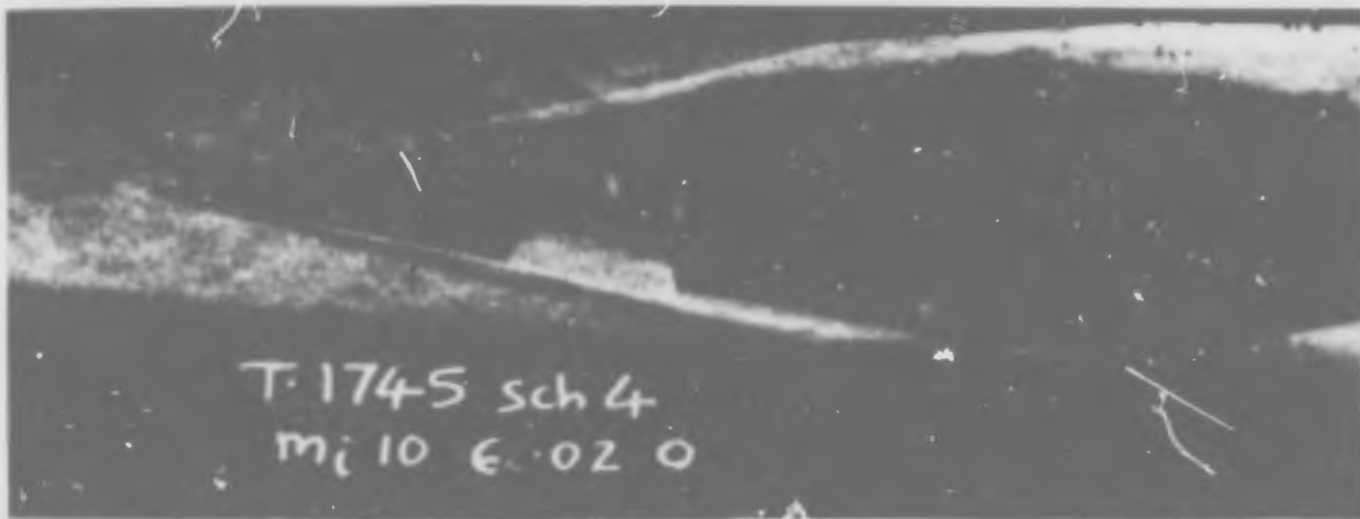
(c) Upstream traverse station.  
Just inside maximum  
shear zone.



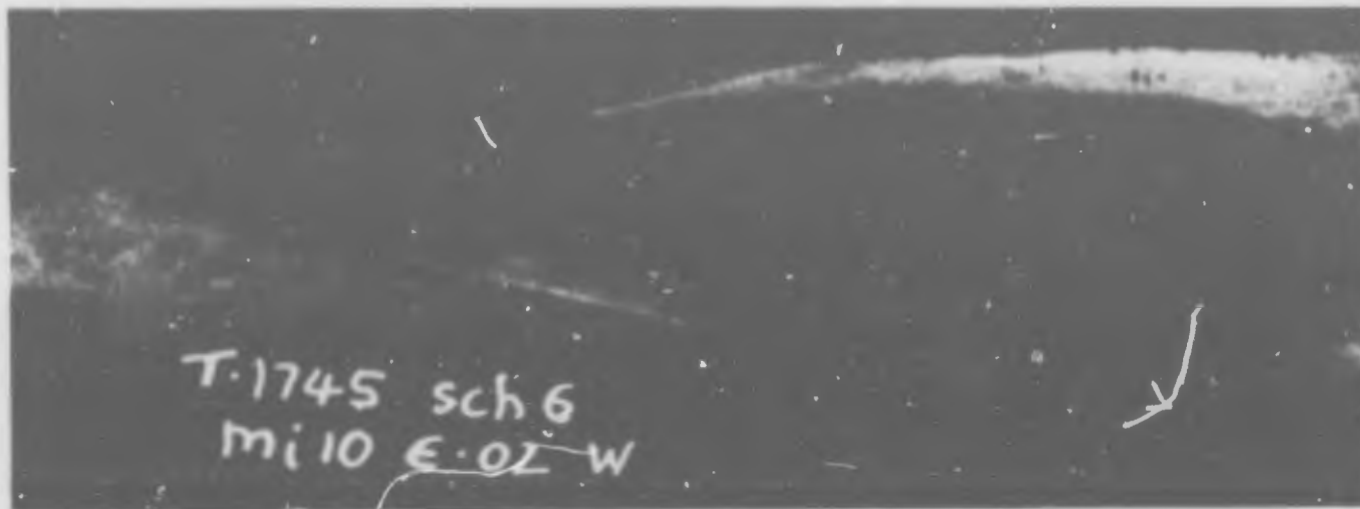
(f) Rear traverse station.  
Close to model surface.

XI I B5-39

Figure 24. Oscilloscope traces obtained during hot-wire surveys of boundary layer downstream of R, with  $m_1 = 10$  microslugs per second, and  $\epsilon_S/L = 0.032$ .



(a) Just outside boundary layer.



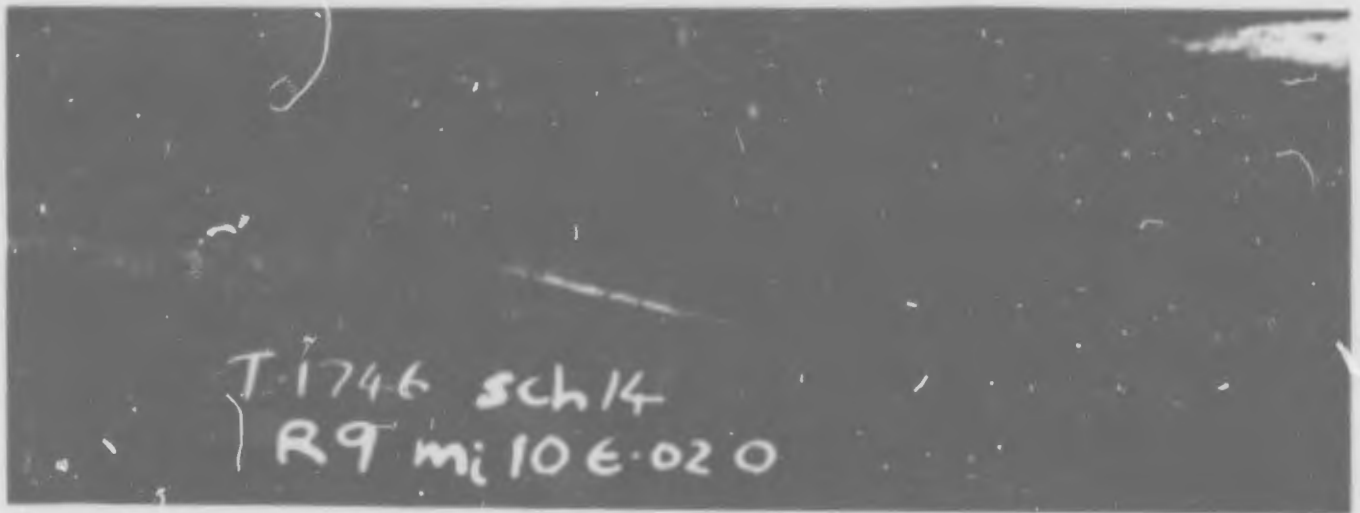
(b) Maximum shear zone.



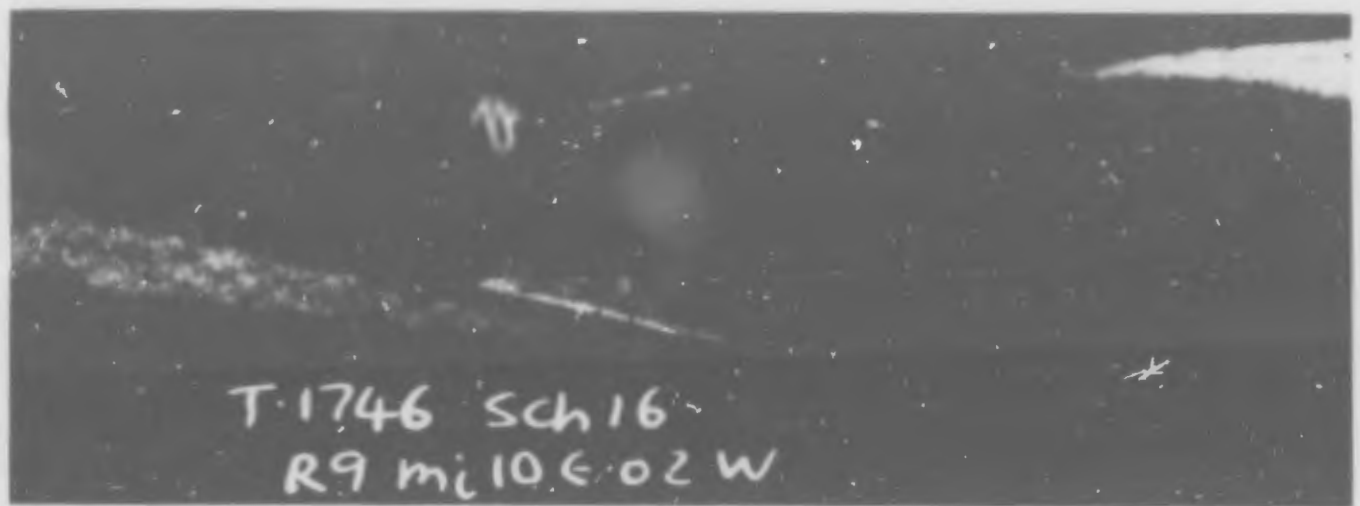
(c) Just inside maximum shear zone.

XII B5-26

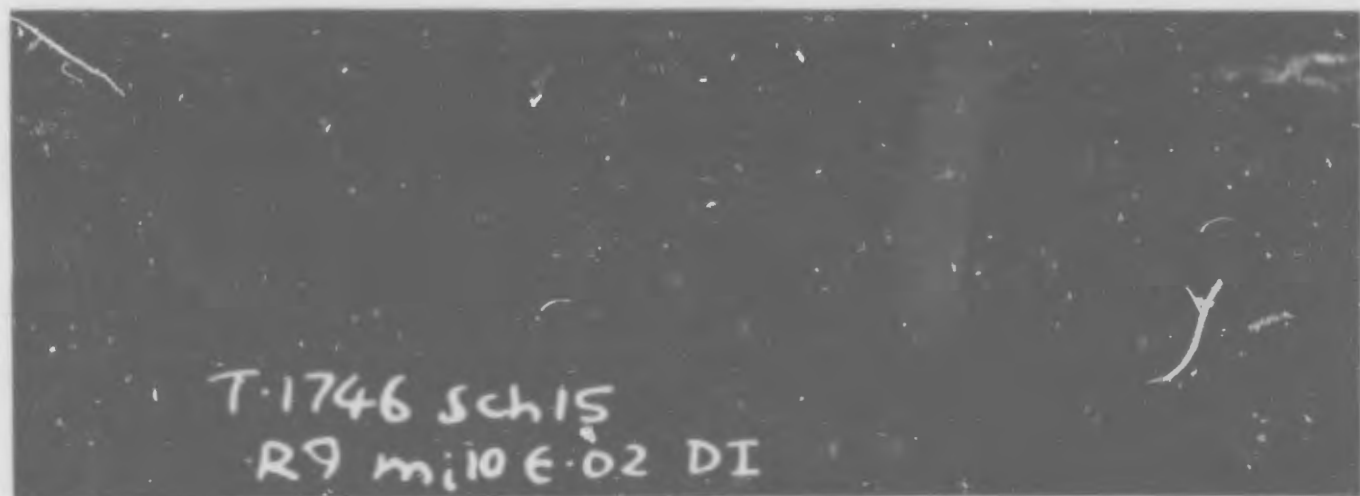
Figure 25. Schlieren photographs of hot-wire traverses of boundary layer downstream of R, with  $m_i = 10$  microslugs per second, and  $\epsilon_s/L = 0.032$ .



(d) Outside boundary layer.



(e) Maximum shear zone.



(f) Close to model surface.

XII B5-27

Figure 25 (continued).